8-9-2012

# Sustainability of CoNi alloy in nanostructured environment through thermogravimetric and corrosion studies

Xu Chen

# R•I•T

# Sustainability of CoNi alloy in nanostructured environment through thermogravimetric and corrosion studies

By

**Xu Chen**

A Thesis Submitted in Fulfillment of the Requirements for the Degree of Masters of Science in Materials Science & Engineering

College of Science
Rochester Institute of Technology
Rochester, NY
Aug 9, 2012

Committee Approval:

---

Prof. K.S.V. Santhanam Date
Thesis Advisor

---

Prof. Changfeng Ge Date
Committee Member

---

Prof. Gerald A. Takacs Date
Committee Member

# Abstract

The interaction of atomized Co, Ni and CoNi with multi-walled carbon nanotubes has been studied by thermogravimetric analysis (TGA) and electrochemical polarization studies. The composites of the above materials have been prepared in different atomic ratios and investigated for examining the spin polarization. The composites have also been sintered at $500^{O}$ to 1000 $^{o}$C in argon atmosphere. The uncomposited metals showed thermal oxidations by TGA in air. The characteristic values for atomized Co, Ni and CoNi are 360$^{o}$C, 500$^{o}$C and 500$^{o}$C respectively. The composited materials showed no thermal oxidations when there is sufficient amount of spin polarizing agent; the spin polarizing agent in this study is multi-walled carbon nanotubes. CoNi alloy alone interestingly showed only one thermal oxidation at 500$^{o}$C. The characteristic oxidation of Co was not observed at 360$^{o}$C suggesting that there is spin polarization occurring due to ferromagnetic metal Ni. These behavioral patterns have been modeled based on the predictions of the density functional calculations in the literature. The prediction is that when a carbon nanotube interacts with Co and Ni the electron distribution is modified in the following ways

$$\text{Co [Ar] } 3d^7 4s^2 \text{ to Co [Ar] } 3d^9 4s^0$$

$$\text{Ni [Ar] } 3d^8 4s^2 \text{ to Ni [Ar] } 3d^{10} 4s^0$$

As a consequence of this spin polarization, the bonding property with oxygen is modified. This spin polarization prevents the thermal oxidation occurring. With an alloy there has been no density functional calculations, however, the experimental results shows that the thermal oxidation can be prevented by compositing it with carbon nanotubes. The absence of spin polarization with graphite composited Co demonstrates that a tubular structure is required for the spin polarization. In a series of measurements made with different quantities of multi-walled carbon nanotubes, it is concluded that one ferromagnetic atom requires five carbon atoms to be surrounded by it.

The TGA experimental data reveals that unlike cobalt composites the nickel composites form at 800$^{o}$C a gaseous compound that is tentatively ascribed to nickel tetracarbonyl. Although cobalt has similar atomic structure, its carbonyl formation does not occur as revealed by TGA.

The electrochemical polarization measurements carried out demonstrates that the Tafel plots showed the corrosion current density for the composited CoNi alloy is two

orders of magnitude smaller than CoNi alloy. This is in agreement with the open circuit potentials of the two systems.

# Acknowledgements

I would like to express my sincere gratitude to all people that helped me during my project. I would like to thank my advisor Dr. K.S.V. Santhanam for providing me the opportunity to purse my masters at RIT and for his continuous guidance all the way long. His valuable suggestions, remarkable ideas and outstanding scientific expertise have helped me immensely to give shape to my exciting research in nanotechnology.

I am also thankful to my committee members, Dr. Changfeng Ge and Dr. Gerald Takacs, for their guidance and help. Dr. Michael Pierce for help with XRD recordings. Thanks are also due to late Prof. M. Illingsworth for permitting to use the high temperature furnaces in his laboratory and Prof. S. Williams for loaning the muffle furnace for a short period.

I would like to thank Ms. Brenda Mastrangelo, Mr. Tom Allston, Mr. John Gallucci and all the staff members of the stockroom for their constant help and support. I am also grateful to all the teachers with whom I interacted as a student.

Finally I express my deepest thanks to my parents and family members for the support and encouragement for which I am very grateful.

# Table of Contents

# List of Tables

# List of Figures

# CHAPTER 1

## 1 Introduction

This thesis is reporting the interaction of CoNi alloy with carbon nanotubes. Since the interaction is with carbon nanotubes, the first part of this chapter will discuss the discovery and the structure of carbon nanotubes. It will describe the differences between graphite, graphene and carbon nanotubes. In the second part of the thesis the distribution of the electrons in the ferromagnetic atoms such as Fe, Co and Ni and the expected rearrangement upon interaction with the carbon nanotubes are discussed. The third part of this chapter will focus on the plan of research and the details of the research.

### 1.1 Overview of carbon nanotube (CNT) and history

Carbon exists in two allotropic forms, graphite and diamond. It has been used for centuries going back to antiquity. In mid 1980, a new allotrope of carbon was discovered that is named bucky balls. This peculiarly shaped molecule led to the investigation of carbon hybridization into a closed ring form. As a consequence, newer forms of carbon such as carbon nanotubes (CNTs), and graphene, were discovered. They are illustrated in Figure 1.1. Furthermore, carbon nanotubes can be of two types, the single-walled and multi-walled, as shown in Figure 1.1a and b respectively. The newer forms of carbon have significantly contrasting properties compared with the older forms of carbon, which are graphite and diamond. In particular, they share in common a hexagonal lattice or arrangement of carbon atoms. In addition, CNTs and graphene occupy a reduced amount of space compared with their older siblings; hence, they are often referred to as reduced-dimensional solids or nanomaterials for short. To give a comparative (order of magnitude) idea of the critical size scales of these nanomaterials, nanotubes are about 10000 times thinner than human hair, and graphene is about 300000 times thinner than a sheet of paper. The typical diameter of nanotubes range from about 1 to 100 nm, and graphene ideally has the thickness of a single atomic layer (~3.4Å). Fundamentally, it is the combination of the reduced dimensions and the different lattice structure that leads to the fascinating properties unique to nanotubes and graphene.

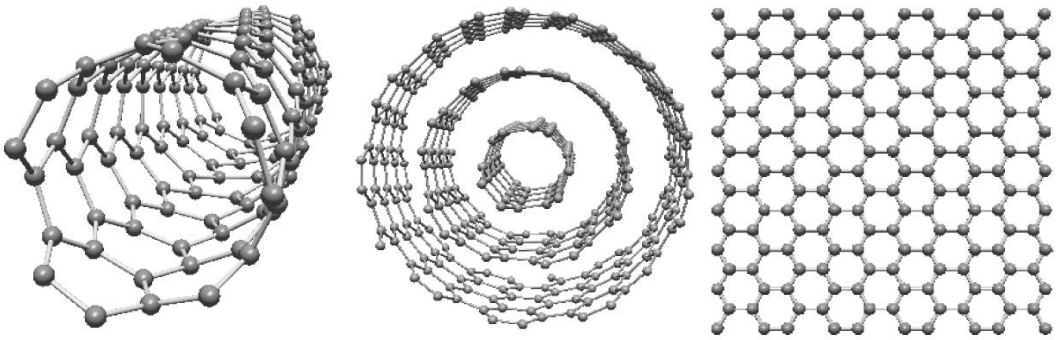

(a) (b) (c)

Fig.1.1 Ball-and-stick models of CNTs and graphene: (a) single-wall nanotube, (b) multi-wall nanotube with three shells, and (c) graphene, which is a single sheet of graphite. The balls (spheres) represent the carbon atoms and the sticks (lines) stand for the bonds between carbon atoms.[2]

While both nanotubes and graphene will be formally studied, the primary focus will be on CNTs. This is because nanotubes have been actively studied since 1991, affording a relatively greater wealth of understanding compared with graphene, which have only recently enjoyed intense scrutiny (since 2005). The excitement and accumulated knowledge regarding nanotubes can be seen in the number of related articles published in the international journals of three major disciplines (physics, chemistry, and electrical engineering), which is reflected in Figure 1.2. Indeed, CNTs have enjoyed a somewhat exponential interest over the past decade, and the current gradual saturation in publications is a sign of the maturity of understanding about their properties. Accordingly, many diverse and novel applications have been explored, as can be seen in Figure 1.3, which is an indicator of the growing applications of CNTs.

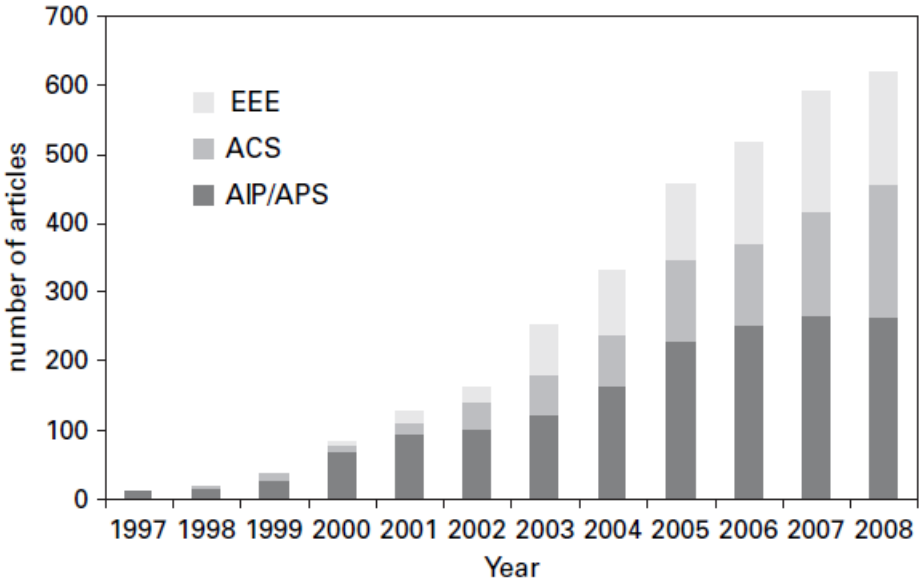


Fig.1.2 Increase in the number of articles in the major international journals with the phrase "carbon nanotube" in the titles. AIP/APS stands for the journals of the American Institute of Physics and American Physical Society respectively. ACS is the acronym for the journals of the American Chemical Society, and IEEE represents the journals of the Institute of Electrical and Electrons Engineers.[2]

This chapter will present a broad historical perspective on CNTs and a brief discussion of the structure and applications.

The developments leading to the discovery of CNTs, or perhaps more fittingly their accidental synthesis, followed a somewhat jagged path of experimental research. Before proceeding any further, the reader should keep in mind that natural deposits of CNTs may well exist in some as yet undiscovered location(s). However, these locations (if they exist) have not been found, or at least no one has been actively searching for them. Moreover, the production of nanotubes may have similarly existed through some inadvertent process for a long time. A case in point is an interesting article by Indian scientists reporting on the synthesis of CNTs from oxidation of specially prepared carbon soot popularly known as *kajal* in South Asia, a substance that has been used as an eye-makeup as far back as the eighth century BC [1]. The historical discussion here will be limited to synthetic or man-made nanotubes that have clearly been identified by undeniable evidence. The origins of these CNTs are ultimately rooted and intertwined with developments of their siblings, carbon

nanofibers and fibers which are hair-like filaments. All these slender structures, namely nanofibers and fibers, can be categorized as filamental carbon for short, with dimensions and morphologies illustrated in Figure 1.4.

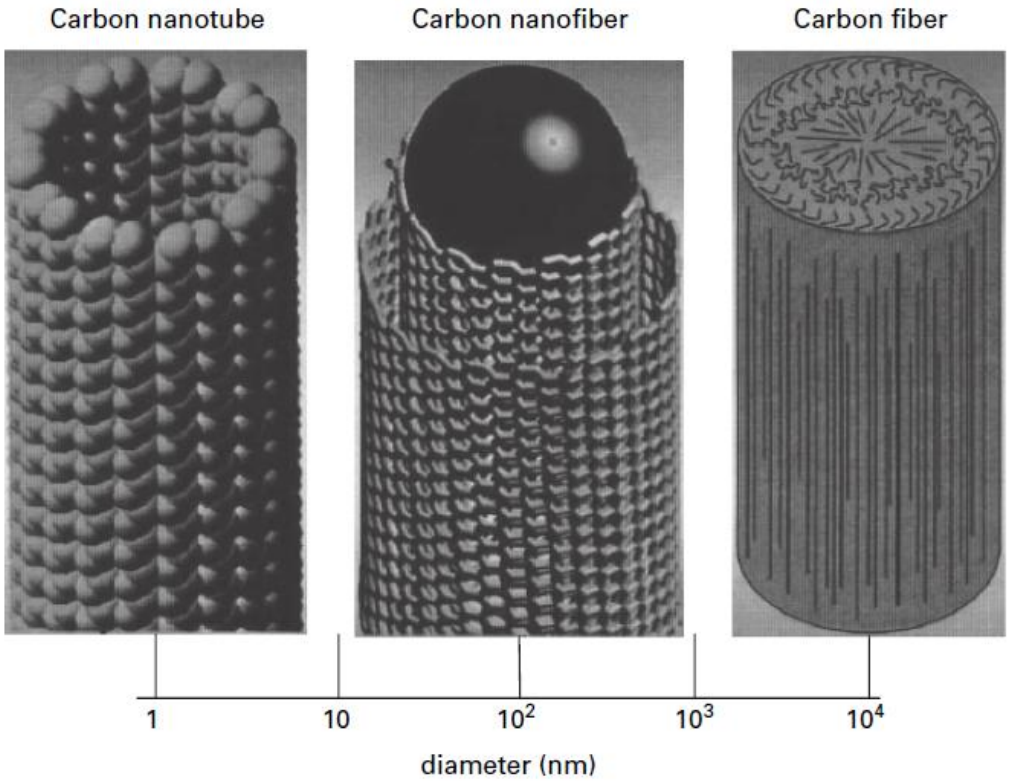


Fig. 1.3 Illustrative morphology and range of typical diameters for different filamental carbon[2]

Historically, the intentional synthesis of carbon fibers can be traced back to the time of Thomas Edison and the beginnings of electrical lighting (late 1800s), when this material enjoyed a growing application as filaments in the commercially successful incandescent light bulb. Indeed, a US patent was issued in 1889 to two British scientists documenting the detailed synthesis of carbon filaments or fibers by what is now known as the chemical vapor deposition (CVD) method (Fig 1.5).

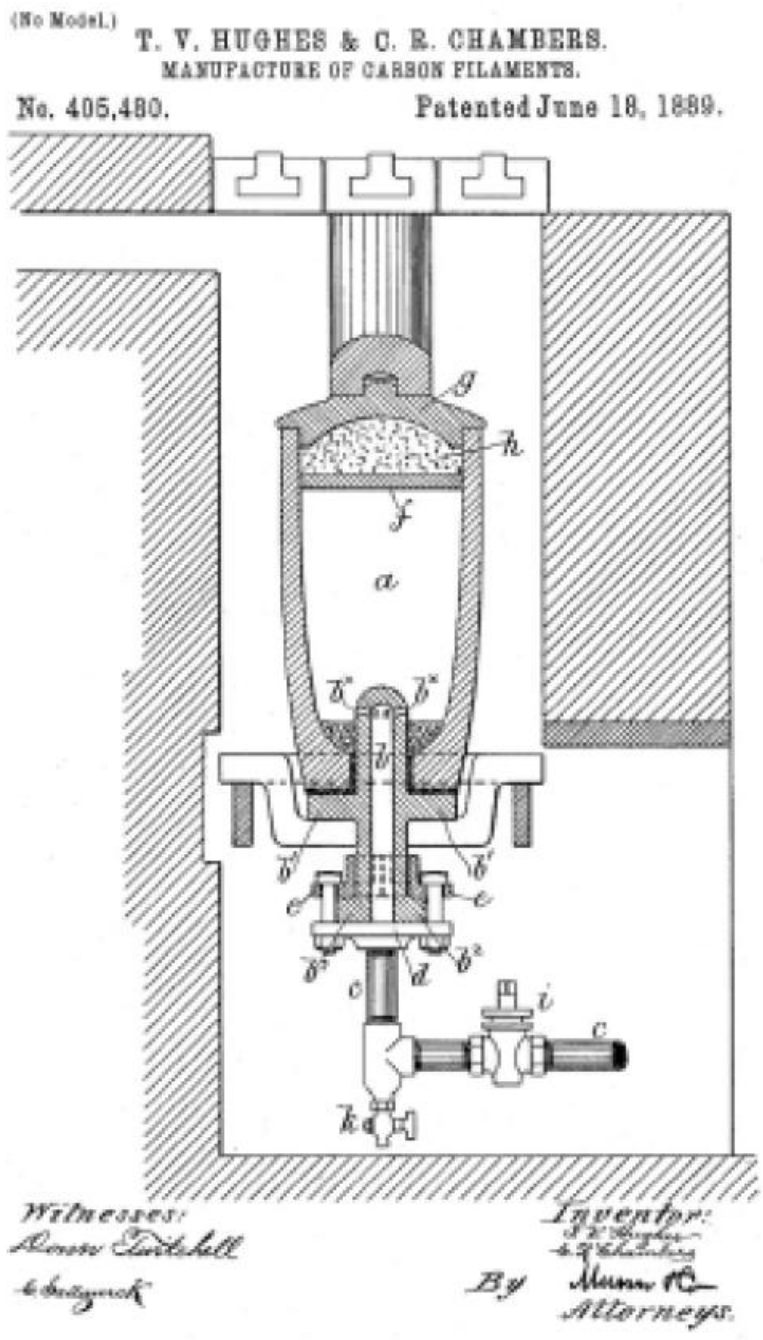


Fig. 1.4 Patent drawing of Hughes and Chambers for the invention of a catalytic high-temperature technique for growing carbon fibers or filaments in a CVD chamber under atmospheric conditions.[2]

Remarkably, the patented CVD recipe, which employs iron to catalyze the thermal decomposition of a mixture of hydrogen and hydrocarbon gases (methane and ethylene are mentioned in the patent as preferable) leading to the growth of carbon fibers, remains the most popular method of synthesizing nanofibers and nanotubes even after a century's worth of research in carbon materials. Some of the highlights in the patent schematic (all labels refer to Fig. 1.5) include a gas outlet (labeled *k*) to

bake out and evacuate any moisture/steam in the chamber before growth and an inlet(*c*) to allow the flow of the gases through a small opening ($b^x$) for subsequent carbon synthesis at high temperatures. The carbon fibers grow from the bottom and the walls of the iron crucible to fill the ~5-inch tall chamber and were mentioned to be of low electrical resistance and high density. At the time, the role of iron as a catalyst was not recognized in the patent. Now we know that iron is a particularly efficient catalyst for filamentary carbon synthesis from methane. A sequence of clay-like layers (f/h) is used to trap the gaseous by-products, which are removed after synthesis. Essentially, the same procedure is employed today for the basic CVD synthesis of nanotubes, typically employing a quartz chamber and patterned iron nanoparticles on a substrate for localized directed growth of CNTs.

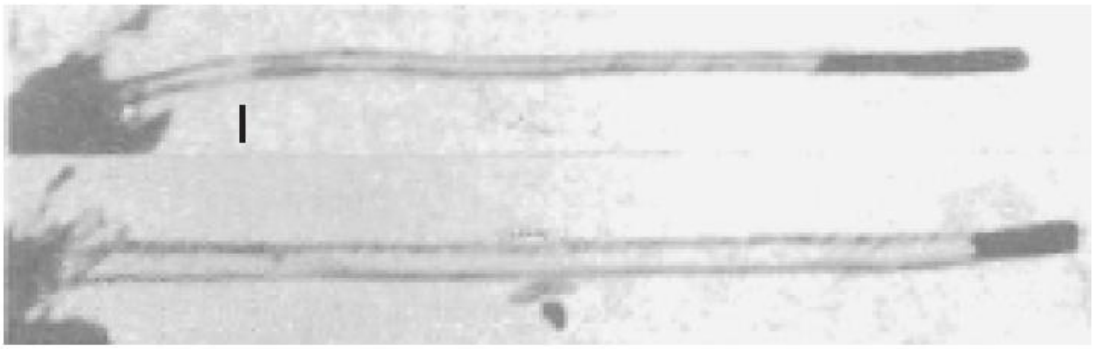

Fig.1.5 TEM images of what appears to be multi-wall CNTs. Adapted from the 1952[5]

With the development of the electron microscope in the 1930s, scientists had a new, extremely useful (and expensive) tool to play with. They immediately began to take a close look at the structure of nature at length scales that had been previously inaccessible. In 1952, Russian scientists reported intriguing transmission electron microscope (TEM) images of filamental carbon structures synthesized from the iron-catalyzed decomposition of carbon monoxide at temperatures in the range of 400-700℃. The TEM images (Figure 1.5) are believed to be the first to show what appear to be (what we now call) multi-walled nanotubes among the other filamental and amorphous carbon products described in the article. They recognized the catalytic properties of iron in facilitating the growth of tubular carbon, and also discussed the initial formation of iron carbide at the base of the tubes followed by the subsequent growth of carbon filaments, a theory which is widely accepted today. British materials researchers (apparently unaware of the Russian article) independently announced

similar filamental observations resulting from thermal decomposition of carbon monoxide in the presence of iron a year later[4].

Inspired by the reports from the Russian and British researchers, Hofer et al. followed up on the suggestion from the former that similar carbon filaments might be produced using cobalt or nickel catalysts instead of iron. In 1955, they were successful in reproducing the synthesis of carbon filaments from carbon monoxide using either Co or Ni catalysts[5]

### 1.2 Spin polarization

Spintronics[6-8] is based on the assumption that information can be carried by the two spin orientations of the conduction electrons. An electron transport process that favors either of the two spins is thus essential toward achieving this purpose. A natural candidate for this spin dependent transport is a ferromagnet, which has a large magnetic moment and spin polarization in the electronic density of states (DOS) near the Fermi level. Among various magnetic materials, transition metals grown on nonmagnetic substrates are widely used to form two-dimensional magnetic thin films[8]. However, for many applications, one-dimensional (1D) nanoscale devices are more desirable. Carbon nanotubes are well studied in many of their physical properties[9] and show great potential as building blocks in nanoscale electronics[9-10]. A combination of carbon nanotube and ferromagnetic transition metals should be promising in providing the required magnetism, dimensionality, and small volume that is relentlessly pursued.

One such combination is a ferromagnetically contacted carbon nanotube achieved by Tsukagoshi et al. [11]. Theirs is a structure consisting of a single multi-walled carbon nanotube electrically contacted by Co. Hysteretic magnetoresistance ratios ranging from 2% to 10% were reported. The presence of the magnetoresistance is attributed to the misalignment of the magnetic moments of the two electrodes (the spin-valve effect). Based on Julliere's model[12], they use a 9% magnetoresistance ratio and a spin polarization of Co at 34%[13] to derive the approximately 14% spin polarization of the electrons traveling the entire length of the nanotube (250 nm) without flipping their spin. The spin-scattering length for the nanotube is then estimated to be at least 130 nm. Without the spin relaxation, the magnetoresistance ratio would have reached as high as 21%. The spin-dependent

transport through the nanotubes or 1D quantum nanowires has also been theoretically studied using the Luttinger liquid model[14]. In a separate theoretical analysis by Mehrez et al.[15], a single-walled carbon nanotube (SWNT) is sandwiched between two electrodes whose ferromagnetic moments point in different directions. An equilibrium Green's function and a simple tight-binding model for the nanotube were used to calculate the spin-dependent conductance at zero temperature and zero bias. Again, a spin-value effect is obtained for the construction. The resistance depends on the relative orientation between the two magnetic moments of the electrodes and can reach a ratio up to 20%. They also show that the transport is dominated by the resonant transmission, which makes the resistance dependent on the length of the nanotube. In particular, if the length of an armchair nanotube is commensurate with (3*N*+1) unit cells along the nanotube axis, the resistance will be reduced by an order of magnitude because of the resonance behavior.

Ideally, a carbon nanotube used for spin-dependent transport should offer as high a magnetoresistance ratio as possible. This can be achieved only if the nanotube itself is made spin polarized. Also, from the practical point of view the device should not depend on the length and type of the nanotube sensitively. These considerations lead us to propose a hybrid construction combining a carbon nanotube and the same transition metals as the electrodes are made of. By traversing the same material the reflection of electrons at nanotube/electrode junction should be significantly reduced [16-17], thus reducing the effect of resonant behavior.

Experimentally, a carbon nanotube based hybrid nanostructure can be achieved either by filling the nanotube with foreign materials in its cavity[18] or by coating the materials on the tube surface. Filling with materials such as transition metals [18-22] or ionic crystals[23] inside carbon nanotubes has been realized. In some experiments, 1D crystal structure actually forms in the cavity of the tube[23]. Coating on the surface of carbon nanotubes can also be achieved with a variety of materials. For example, titanium can form stable and continuous structures on the nanotube surface [24-26].

### 1.3 Previous work

Rawat, Gudyaka and Santhanam[27]. have researched the thermal oxidative behavior of atomized iron and atomized cobalt in the presence of MWCNT. The TGA showed the atomized iron thermal oxidation started at about 500℃ that was absent when the atomized iron is sintered with MWCNT. The thermal oxidation of iron or

cobalt in sintered samples requires collapsing of the MWCNT. This thermal oxidative shift was interpreted as due to the atomized iron or cobalt atom experiencing extensive overlap and confinement effect with MWCNT causing a spin transfer. This confinement effect was suggested to produce a transformation of iron from the outermost electronic distribution of $3d^6 4s^2$ to an effective of $3d^8 4s^0$ and for cobalt $3d^7 4s^2$ to $3d^9 4s^0$ producing spintronics effect.

Joshi, Gupta and Santhanam[28] have demonstrated that sintered samples of cobalt-MWCNT has an extremely low corrosion rate [corrosion rate: mils per year (mpy) for Co:MWCNT=1:1 was 1.211, Co:MWCNT=1:2 was 0.977 and compared to Co was 2.456]. This material has cobalt in a highly shielded environment of MWCNT that give it a protection from the thermal oxidation up to about 800℃.

Fagan and Mota[29] have investigated the interaction of an iron atom with a single-wall carbon nanotube using spin-polarized total-energy first-principles calculations. It was shown that when the atom interacts with the tube from outside, a $3d^7 4s^1$ effective configuration was obtained and the total magnetization was close to the atomic value. For the inside case, as a consequence of higher hybridization and a confinement effect, the magnetization decreases and the finally obtained effective configuration was $3d^8 4s^2$.

### 1.4 Applications

Ever since the discovery of carbon nanotubes by Iijima[30] innumerable number of attempts were made to find applications. CNTs have been found to be useful as an electrode material in sensor applications[31-49], electronic devices[50-54], and high tensile strength material[55-59]. The power of carbon nanotube in chemical and electrochemical applications has been recently reviewed[60]. The carbon nanotube is a highly pi conjugated molecule that enables covalent attachment of chemical groups such as fluorine, carbine (2+1) cycloaddition, hydrogenation, radical additions, ozonolysis, electrophilic additions and grafting of polymers. Several Vanderwaals type of interaction that is typical of adsorbing systems has also been discussed in the literature[61] where bio molecules are forming functional assemblies through integration with carbon nanotubes. Insertion of metals inside the carbon nanotubes has been of interest in the context of their storage and in developing nanowires. In this category, density functional calculations [62,63] have yielded results suggesting that when the metal atom is in the peripheral of the nanotubes it produces an increased

hybridization. For cobalt atom with the outermost electronic configuration of $3d^7 4s^2$, the effective hybridization results in $3d^9 4s^0$ [64-66] through the interaction with carbon nanotubes.

Cobalt and cobalt alloys are unique in that they can absorb stress to a higher absolute temperature than other ferromagnetic metals[67-68]. In addition it has an excellent resistance to thermal fatigue and can be welded[69] with a low resistance to corrosion and wear[70], cobalt requires to be alloyed with chromium and molybdenum to improve its performance as prosthetic parts such as hip, knee or dental partial replacement[71].

### 1.5 Purpose of the thesis

The purpose of this thesis is to study the interaction of ferromagnetic metals and their alloys with carbon nanotube from the point of view of sustainability. This subject is important in relation to the contact resistance and nanoelectronics. In addition, the ferromagnetic metals are used as catalysts in a large number of industrial processes. Their sustainability has been a challenging problem. At RIT, sustainability of atomized iron and cobalt has been investigated in the earlier studies [27, 28]. The present thesis has been devoted to the composites of atomized nickel and its alloy CoNi with multi-walled carbon nanotubes. The first Chapter discusses the history and developmental aspects of carbon nanotubes. A short review of the literature provides an insight into metallic interactions with carbon nanotubes. The second chapter gives the experimental techniques employed in the present study and the material sources. The third Chapter discusses four models for the spin polarization of the ferromagnetic atom. This modelling is an important part of the thesis that evolves a thermogravimetric method to distinguish the spin polarization that enables to understand the thermal stability of composited Co, Ni and CoNi alloy. The spin polarization studies lead to the conclusion that a tubular nature of the carbon nanotube is required for spin polarization in the ferromagnetic metal. In addition, for every one ferromagnetic atom five carbon atoms are required for complete spin polarization.

The fourth chapter discusses the experimental thermogravimetric results of the above materials. Here the materials that are unsintered and sintered are used. The sintered materials are later constructed into electrodes. The final Chapter discusses the sustainability of the composited alloy with multi-walled carbon nanotubes by electrochemical polarization studies. Chapter 6 gives the conclusions and possible future work arising out of this thesis.

# CHAPTER 2

In this chapter, the experimental details are given. It discusses, the materials used and the preparative methods employed. It also contains the instrumental details that are relevant to this work.

## 2.1 Materials and preparations

Table 2-1 Experiment equipment and model

| Instruments and equipment | Manufacturers |
|---|---|
| TGA | TA(Delaware) |
| FTIR | Biorad Excalibur Series FTS 300 |
| XRD | Indigenously Fabricated Dr. Pierce |
| Electrochemical workstation | Gamry Instruments |

Table 2-2 Experiment materials

| Name | Model or grade | Manufacturers |
|---|---|---|
| Nickel powder, spherical | 99.9%-325MESH | AEE(Atlantic equipment engineers) |
| Cobalt powder, spherical | 99.9%-100MESH | AEE |
| MWCNT | 99.9% | HELIX Material Solutions |

**Material Compositions**

The compacted ferromagnetic metal or its alloy made of Co and Ni are sintered at 500 -1000 $^{o}$C for six hours in argon atmosphere in a muffle furnace before use. The material compositions are given at the appropriate places in the thesis.

## 2.2 Thermogravimetric analysis (TGA)

Many substances during the process of heating or cooling tend to have quality changes in addition to the thermal effects; the size of the change is dependent on the temperature, the chemical composition and structure. Therefore, the use of the

material changes in the heating or cooling process can be used to identify different substances. This method is called thermogravimetric analysis; it is analysis of the weight of the sample as a function of time or temperature and the curve is known as the TGA curve. TGA curves show the changes in sample mass in the longitudinal axis; the horizontal axis represents either time or temperature. Fig. 2-1-shows the vertical axis with the specimen weight loss expressed as a percentage while Fig. 2-1-b gives the vertical axis as the percentage of sample.

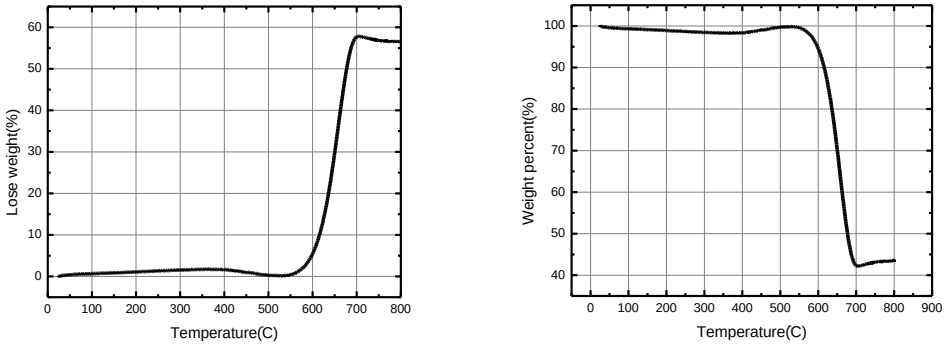


(a) (b)

Fig.2-1 Co:MWCNT=0.5:1 sample TGA curve.

**2.2.1 Thermogravimetric analyzer**

The thermogravimetric analysis is generally done by either in the static or dynamic mode. The static mode uses a sample heating at each selected temperature to constant weight for examining the shape of the temperature plot (Fig.3-1-a and Fig.3-1-b). In dynamic mode, the heating process is continuous where heating and weighing are done; the temperature changes according to the nature of the sample. The static method has the advantage of high accuracy because it measures small changes in the weight loss while the disadvantage is long time of measurement. The dynamic mode has the advantage of automatically recording and working closely together with the differential thermal analysis or comparative analysis; the drawback is that it involves a tiny mass change.

The thermogravimetric analysis is based on either thermal balance or spring scale.

1. Thermobalance type

The current thermogravimetric analysis instrument uses more heat balance style. The mass changes of the sample are measured by either variable counterpoint or zero measurement. The deflection method is to tilt the balance beam so that the sample

quality is proportional to the mass change. It uses a differential transformer to detect the inclination for automatic recording. The zero method uses the differential transformer, optical with electrical contact detection balance beam, tilt spiral coil roll in the balance system in a permanent magnet, resulting in tilting the balance beam to reset. By using the force applied to the permanent magnet, the mass change of the specimen is calculated from the current flow through the spiral coil. This current change is recorded in the TGA curves.

2. Spring balance type

The principle of spring balance is based on Hooke law; the elastic stress of spring and strain are related by a linear relationship. Normally, the elastic modulus of spring materials change with temperature, and it is easy to have an error due to this factor; so small temperature changes in the quartz glass are measured by annealed tungsten.

Quartz glass spring because of its minimal frictional impact and vibration is difficult for attenuation, and therefore difficult to operate. In order to prevent the change of the thermal radiation and convection in the furnace affecting the modulus of elasticity of the spring, the spring is equipped with a circulating constant temperature bath. With the spring balance method, the extent of spring stretching to weight relationship is used, so we can use the altimeter readings or differential transformer to convert the electrical signal for automatic recording.

### 2.2.2 Experimental method of thermogravimetric analysis

Currently the most widely used thermogravimetric analysis is an automatic recording of weight and temperature and it easily combines with other thermal analysis techniques.

1. Correct parameters

Before the experiment, the weight correction recorder (such as the spring stretching, balance beam tilt, flow through the spiral coil current, etc.) should be used to correct the changes in the sample mass ratio in TGA. Usually the instrument is calibrated when shipped, if necessary, it should be re-calibrated.

2. Experimental procedure

(1) Pretreatment of the sample, weighing and filling

The specimens were pre-pulverized and dried. Weighing in thermogravimetric

analysis should be accurate; if the sample is small, a higher demand of accurate weighing is required. The sample is accurately weighed into the crucible; the loading process is an important part of differential thermal analysis.

(2) Heat rate selection

The heat rate selection should ensure the baseline is smooth. The quality changes in the sample under a certain temperature range of the instrument should be able to get the quality changes significantly in the TG curve.

3. Factors of the TGA curves

The TGA curves are mainly due to the impact of internal and external causes. The internal factors depend on the intrinsic characteristics of the sample; external factors will depend on the instrument structure, operation, environmental conditions and other experimental factors. The following focuses on the impact of external factors.

(1) Changes in buoyancy and convection

Buoyancy changes due to the surrounding gas of the sample may involve change of temperature which may led to the mass change. The buoyancy at 573K is about 1/2 of the buoyancy at the room temperature, and at 1173K it is reduced to about 1/4. When the heated parts of the sample plate and the support beam are larger, buoyancy change is particularly significant.

Convection in the TGA experiment is also an important factor, but difficult to eliminate. The balance system is in room temperature while the sample is at a high temperature, it will cause convection because of the temperature difference and this certainly affects the accuracy of the measurement. To this end, the heat shield panels or cooling water devices between the sample and the balance will be used to reduce or eliminate the effects of convection. Figure 2-2 shows three different positions, the horizontal position (a) is better.

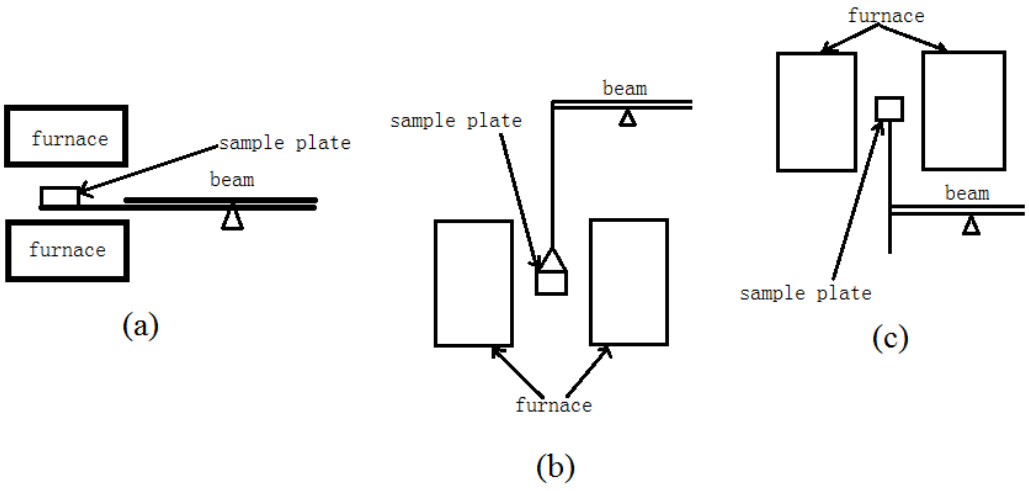


Fig.2-2 Three different positions of beam, sample plate and furnace[72]

Not only buoyancy decreases, convection and different other modes affect the measurement in addition to the sample volume. Usually based on the low temperature part of the TGA curves, the weight of the sample before and after test is compared to determine the real weight change.

(2) Re-condensing of volatile and the temperature measurement

The heating process can decompose or volatile the product samples; volatiles tend to rally in support of the low-temperature part of the sample plate, resulting in errors in the thermogravimetric analysis.

The measurement error is always part of the thermal analysis. Thermocouple solder joints in thermogravimetric analysis, often do not contact the sample. In isothermal temperature increase, the temperature distribution is due to the uneven distribution of the ambient temperature of the sample that results in disorder in the reaction process. This temperature error is more serious. To this end, the International Thermonuclear Committee for Standardization agreed upon the use of nickel or other strong magnetic bodies for keeping the sample in a magnetic field.

Other factors

The results could be affected by the nature of the gas and by the existence of natural convection. In the heating process, the volatile products tend to have internal diffusion that will cause the weight loss-time lag phenomenon. In addition, the vibration can also affect the curve shape of the TGA and hence the thermogravimetric analysis should be done on a shock proof table.

### 2.2.3 Applications of thermogravimetric analysis

Thermogravimetric analysis could be used to test the materials that change their weight during heating or cooling process, in the differential thermal analysis for the accurate identification of these substances.

TGA curves of the magnetic materials require to be corrected for the calculation of the activation energy.

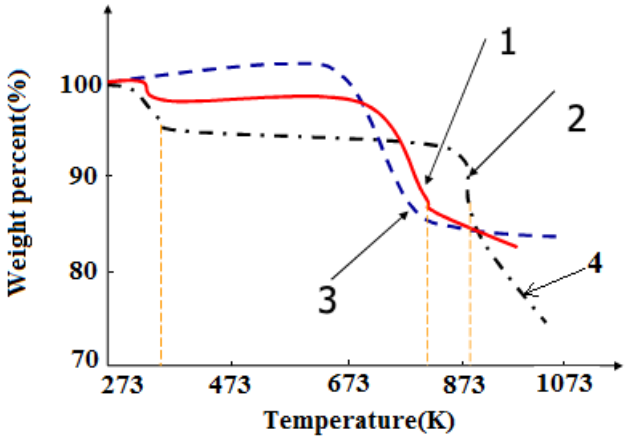


Fig. 2-3 TGA curves of kaolinite, hectorite, and mixtures: 1 - kaolin (weight loss 8.9%); 2 - hectorite (weight loss 6.3%); 3 - pure kaolinite (weight loss 12.4%,); 4 - pure hectorite (20.6% weight loss)[72]

TGA curves of kaolin, hectorite, and their mixtures are shown in Fig. 2-3. Because of different dehydration temperatures, Kaolinite and montmorillonite are easy to distinguish. Kaolinites lose all water structure at 833K; the loss of water of about 12.4%. Hectorite lost its adsorbed water around 373K, the loss of water is about 10%, at 903K; the structural water, weight loss is 10.6%. The total water loss is about 20.6%. We can see from Fig.2-3, curves 1, 2, the dehydration temperature of the two minerals are different. We can calculate percentage of kaolinite and hectorite in a mixture by the weight loss rate of each mineral (kaolinite about 71%, the hectorite about 29%).

Usually we combine TGA, DSC and DTA for qualitative analysis of the clay minerals to avoid errors.

1. Determination of the strong magnetic materials' Curie point

Thermogravimetric analysis can be used to determine the Curie point of the strong magnetic materials. Fig2-4 shows the results of determination of the Curie point of the five kinds of strong magnetic materials. The figure shows the measured temperature very close to the literature value. It can make use of precise Curie point

temperature of these substances to correct the thermogravimetric analysis.

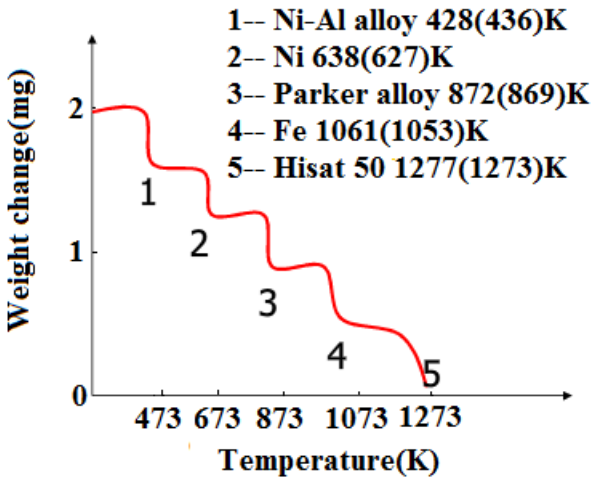


Fig.2-4 Curie points of different strong magnetic materials[72]

Determination of the activation energy and reaction order:

Freeman and Carroll[72] method can be used to determine the thermal decomposition reaction and the activation energy from the TGA curve.

Assume that one of the reaction products is a volatile substance, then a solid thermal decomposition reaction is represented as :

(2-1)

A loss rate of reactive substances can be expressed as

— (2-2)

*X*——Concentration of substance A (mol•$L^{-1}$);

*K*——Reaction rate constant ;

*n*——Reaction order.

Let Arrhenius equation — go into equation (2-2), we can get:

— — (2-3)

*f*——Frequency factor ;

*E*——Activation energy (J/mol);

*T*——Absolute temperature (K)

*R*——Gas constant.

Differential equation (2-3) in logarithmic form, and then get points:

(2-4)

(2-5)

Let equation (2-5) divide by on both sides:

(2-6)

For to use the equation (2-6), we need to apply the relationship between number of moles and mass:

(2-7)

(2-8)

$N_o$——Number moles of A before reaction (mol);

$N_a$——Number of moles at time (mol);

$W_c$——Overall quality changes at the end of reaction (%) ;

$W$——Quality changes at the time t(%) ;

$W_r$——Weight loss percent (%)

Let equations (2-7) and (2-8) go into equation (2-6), and we can get:

(2-9)

If is the vertical axis, is the horizontal axis mapping to obtain the activation energy E from the slope of the line in the Figure, the reaction order n can be obtained from the intercept.

**2.3 Fourier transform infrared spectroscopy (FTIR)**

The vibrational spectra are used for the study of materials, and gives information on the vibrations of the molecule or atoms, resulting in the absorption of light. If we use a monochromator to disperse the radiation, simultaneous measurement of the radiation of different wavelengths could be done which will enable to generate the absorption spectrum. If the light source used is the infrared range of wavelengths, namely 0.78 to 1000μm is the infrared absorption spectrum.

2.3.1 IR spectra and the representation

When continuous infrared light is used to activate a molecule and the vibration

frequency of atoms in a molecule is exactly the same with the exciting infrared light the it causes resonance absorption. It will decrease the light transmission intensity. Therefore, by plotting the wavelength (or wave number) against the light transmittance, an IR spectrum can be obtained. Fig. 2-5 is the FTIR curve of the Co after it is oxidized in the furnace (500 $^{c}$o. for 5 hours); because it is molecular resonance absorption so it is called the absorption spectrum. The spectrum shows horizontal axis as wavelength (μm) or the wave number ($cm^{-1}$) and the vertical axis as transmittance% (sometimes absorbance). The absorption in the infrared spectra is referred to as band, not as peak.

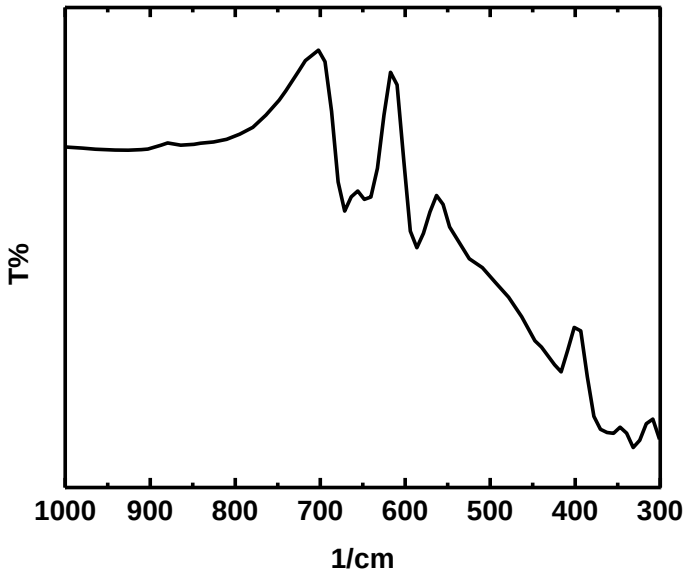


Fig. 2-5 FTIR curve of Co after 550 $^{o}$C 5 hours [Present work]

In general in infrared spectra, the wavelength is in the infrared region in the range of 2.5 to 25μm (400 ~ 4000cm-1). A vast majority of organic and inorganic compounds absorb in this wavelength range.

2.3.2 The characteristics of IR spectra

IR spectra generally reflect the four features in the spectrum and they must be used in the interpretation. They are

（1） Number of bands: we must first analyze how many bands are there in the infrared spectrum

（2） Location of absorption bands: Due to the vibration of each group having characteristic vibrational frequencies, the IR spectrum shows specific absorption band

positions at a selected wavenumber $cm^{-1}$. In the identification of compounds, the band position (wave number) is often the most important parameter. $OH^-$ absorption wavenumber is located at 3650~3700$cm^{-1}$ and the absorption of water molecules occur at a lower wave number of 3450$cm^{-1}$.

（3） Shape of the band: In the analysis of compounds in the pure form (crystal, liquid, gas can be analyzed), the spectra are relatively sharp and in good symmetry. If the mixture is sometimes having overlapping bands resulting in the widening, then the symmetry is destroyed. With Crystalline solid material, the integrity of the crystal affects the band shape. Figure 2-6 is the IR spectrum of crystalline $SiO_2$ (quartz) and amorphous $SiO_2$. Seen from the figure of Si-O bond vibration frequency range of 900 ~ 1500$cm^{-1}$ and 650 to 800$cm^{-1}$. The quartz crystal has two sharp strong absorption bands at 780$cm^{-1}$ and 690$cm^{-1}$. Quartz glass is having one at 800$cm^{-1}$ and another one at 680$cm^{-1}$ that is broad and weak.

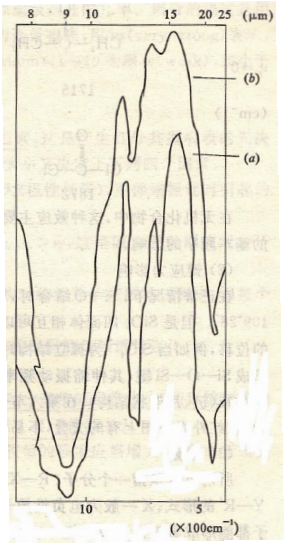


Fig.2-6 FTIR of $SiO_2$: (a) crystal, (b) non-crystal[72]

（4） Intensity of the bands: Based on the strength of certain compounds, their absorption is large or small and hence the transmittance of infrared radiation is small or large. Just like in ordinary visible light absorption spectroscopy, here also the absorption obeys the Beer-Lambert's law expression and using the following formula:

– – (2-10)

*A*——Absorbance or molar absorption coefficient；

$I_0$ , *I*——Intensity of the incident and transmitted light；

*T*——Transmittance，$I/I_0$；

*b*——Thickness of the sample(cm)；

*k*——*Absorption* coefficient($cm^{-1}$).

### 2.3.3 Factors of the IR spectra

Degrees of Freedom- molecular vibration and the IR bands.

In theory, each vibrational degrees of freedom of the molecule will be reflected in the absorption band in the IR spectrum. However, due to the resonance absorption, the molecular dipole moment changes; some of the same vibration frequencies are degenerate and hence the infrared spectrum of absorption bands is often less than the theoretical number of vibrational degrees of freedom. But on the other hand, due to the presence of overtone also in the fundamental frequency it generates multiples of absorption bands, namely $2\nu_1$ $2\nu_2$ ... at two different frequencies; the difference may be found as the sum of $\nu_1 + \nu_2$ or difference in frequency of $\nu_1$-$\nu_2$. However, the transition probability is small here; the band intensities are often weak in the infrared spectra.

**Factors that affect the band position (displacement)**

The characteristic frequency of the vibration of the groups can be calculated according to the interatomic bond force constants. The groups and the surrounding environment will occur in the mechanical and electrical coupling, making the force constants that are variable. Due to the presence of varying degrees of coupling, the characteristic frequency of the groups has changed, making the band to shift; this change in turn affect molecules in the adjacent groups.

Displacement factors affect the band in general that can be summarized in the following aspects:

（1） Inductive effect

It is caused by polarity of the covalent bond with the substituent electronegativity difference arising from the electrostatic induction effect of varying degrees, causing changes in the charge distribution in the molecule, thus changing the bond force constants, so that the vibration frequency changes-it is known as the inductive effect. In inorganic compounds, this effect is mainly reflected in the combined groups.

(1) Bond stress

(2) Hydrogen bonds

(3) Impact of the materials' state

In the gaseous state, due to the intermolecular distance, the interaction is negligible. In a liquid, the intermolecular interaction is very strong and some compounds will form hydrogen bonds. As for the solid state that is in a crystalline state, due to the order of the crystal, it strengthens the interaction between the vibrations in the molecule.

**2.3.3.1 Factors of the band intensity**

The intensity of absorption bands in the infrared spectrum depends on the dipole moment and energy level transition probability.

Changes in the dipole moment: The dipole moment change during the vibration process is a major factor in determining the strength of the base spectrum, which is a prerequisite for infrared resonance absorption. The size of the instantaneous dipole moment was decided by the following four factors: the electronegativity of the atom, the form of the vibration, the symmetry of the molecule, coupling between the double frequency and the base frequency vibration (known as Fermi resonance).

Energy level transition probability: this directly affects the intensity of the bands, the bigger probability results in bigger intensity of the bands. There is the proportionality relationship between sample concentration and the intensity of absorption bands, which is the basis for a quantitative analysis.

**2.3.3.2 Division of the infrared spectral band**

The infrared spectrum is generally divided into two types:

（1） Characteristic bands of area sometimes referred to as the functional group area, which refers to the vibration frequency in the infrared spectrum between 4000~ 1333cm$^{-1}$ absorption bands.

（2） Fingerprint band area, it occurred in 1333 to 667cm$^{-1}$ vibration absorption, vibration of the group of inorganic compounds mostly produced in this wavelength range.

**2.3.4 Characteristics of the infrared spectroscopy**

Compared with other material structure test methods, infrared spectroscopy has the following high characteristics; it is not limited by the physical state (gaseous,

liquid and solid can be determined) and is independent of the amount of the sample; easy to operate with a high test speed and good reproducibility. It requires authentic spectra for comparison.

However, infrared spectroscopy has its limitations in sensitivity and accuracy; when the content of sample is less than 1%, it is difficult to detect. The interpretation of qualitative and quantitative analysis requires known standards. More importantly most of the band positions are concentrated in the fingerprint region; the bands overlap frequently and are hard to distinguish them.

### 2.4 XRD

X-Ray diffraction spectrum was recorded using Philips XRD spectrometer using CuKα1 radiation source. The 2θ reflections range was set from 15 to 90 degrees. XRD was used mainly to characterize the CoNi alloy. Figure 2.7 give the alloy showing 2 theta reflections at $57.9^{o}$, $61.7^{o}$, $66.7^{o}$ and $77.5^{o}$.

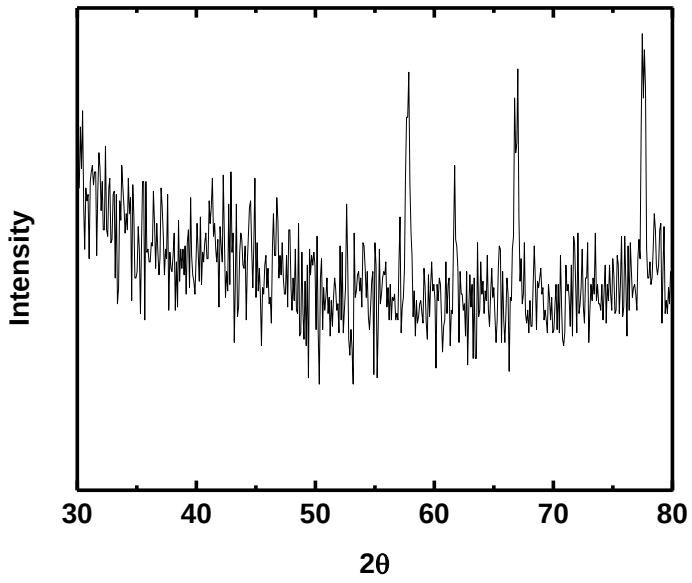


Fig 2-7 XRD curve of NiCo=1:1 after TGA [present work]

### 2.5 Tafel plot

The Tafel plots are recorded using a three necked electrochemical cell that is fitted with a working electrode, saturated calomel electrode (SCE) and a platinum or carbon rod counter electrode. The working electrode used in these measurements is shown in Figure 2.8. Gamry Instrument is used for the potentistatic polarization. The Tafel plots

were both manually and software analyzed to obtain the exchange current density and the open circuit voltage.

It is a technique used to obtain an accurate estimate of the corrosion rate of a metal in a solution. All the electrodes are connected to a device called a potentiostat. A potentiostat allows you to change the potential of the metal sample in a controlled manner and measure the current flow as a function of potential. When the potential of a metal sample in solution is forced away from $E_{oc}$, it is referred to as polarizing the sample. The response (current) of the metal sample is measured as it is polarized. The response is used to develop a model of the sample's corrosion behavior.

The value of either the anodic or catholic current at $E_{oc}$ is called the corrosion current, $I_{corr}$. $I_{corr}$ is used to calculate the corrosion rate of the metal. $I_{corr}$ cannot be measured directly. However, it can be estimated using electrochemical techniques.

An electrochemical reaction under kinetic control obeys the Tafel equation.

(2-10)

I is the current resulting from the reaction.

$I_0$ is the exchange current (constant).

E is the electrode potential.

$E^0$ is the standard potential

β is the reaction's Tafel constant (constant for a given reaction).

The Tafel equation describes the behavior of one isolated reaction. In a corrosion system, we have two opposing reactions anodic and cathodic. The Tafel equations for both the anodic and cathodic reactions in a corrosion system can be combined to generate the Bulter-Volmer equation.

(2-11)

*I* is the measured cell current in amps.

*Icorr* is the corrosion current in amps.

*E* is the electrode potential.

*Ecorr* is the corrosion potential in volts.

*βa* is the anodic beta Tafel constant in volts/decade.

*βc* is the cathodic beta Tafel constant in volts/decade.

The numerical result obtained by fitting corrosion data to a model that generally gives the corrosion current.

(2-12)

*CR* is the corrosion rate.

*Icorr* is the corrosion current in amps.

*K* and *A* are constants that defines the units for the corrosion rate.

*EW* is the equivalent weight in grams/equivalent.

*d* is the density in grams/$cm^3$.

*A* is the sample area in $cm^2$.

**2.6 Cyclic voltammetry (CV)**

CV is an electroanalytical method in which the current response of a small stationary electrode in an unstirred solution is excited by a triangular potential waveform. The current is measured as a function of potential. CV is used to study fundamental oxidation and reduction processes in various media, absorption process on surfaces, electron transfer mechanisms of chemically modified electrodes and for determining charge storage capacity of potential battery electrode materials. The electroanalytical cell consisted of three electrodes, immersed in solution containing an analyte. The working electrode was made of the Ni-Co-MWCNT, a saturated calomel electrode was used as the reference electrode and platinum plate electrode was used as the counter electrode. We used the glass tubes filled with the samples as the working electrodes (see fig2-8). The exposed area of the working electrode was around 3.5$mm^2$. Gamry instruments framework version 3.11 software was used for CV.

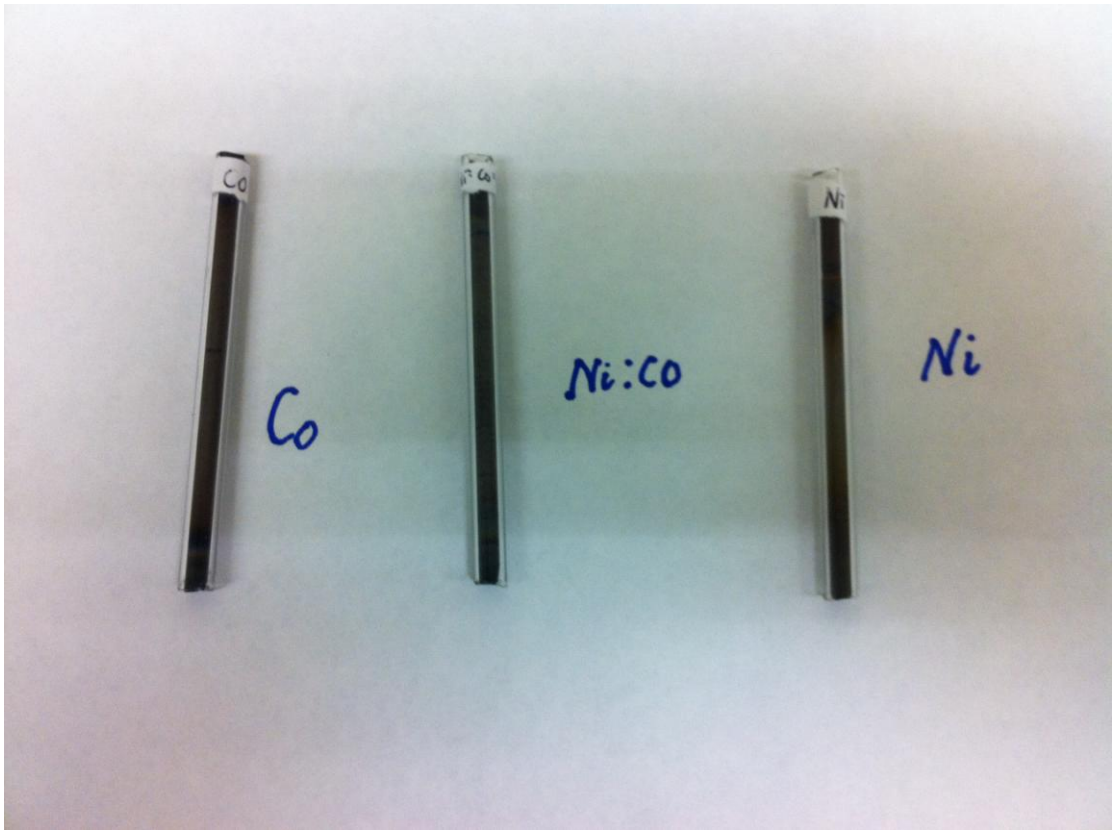


Fig2-8 Co, NiCo alloy and Ni working electrodes

# CHAPTER 3

## 3 Theoretical models

The interaction of multiwalled carbon nanotubes has been studied by a number of workers previously[9,15,19,27-29,55,60]. A detailed theoretical calculation of the interaction was done by Fagan et al[62,63] using density functions. The density functional calculations showed that the type of interaction is dependent on the position of the ferromagnetic metal with respect to the carbon nanotube. Two extreme situations are predicted. One when the ferromagnetic metal is outside the carbon nanotube, the metal behavior is predicted to be unaffected. In the other situation, when it is interacting strongly, the ferromagnetic metal is surrounded by carbon atoms and affecting the normal reactivity. This situation is to cause spin polarization in the ferromagnetic atom. The ferromagnetic atoms considered here are Fe,Co and Ni. The electronic configurations of these three metals are Fe [Ar] $3d^6 4s^2$, Co [Ar]$3d^7 4s^2$ and Ni [Ar]$3d^{10} 4s^0$. The density functional calculations have shown that when carbon nanotube interaction is strong, spin polarization occurs and the new electronic

configurations are Fe [Ar] $3d^8 4s^2$, Co [Ar]$3d^9 4s^2$ and Ni [Ar]$3d^{10}$ $4s^0$. On the basis of this new electronic configuration, it would be interesting to study the binding property of oxygen to the ferromagnetic metal. This is important because the oxidative degradation of metals at high temperature has been of great concern in terms of sustainability. Besides alloys like CoNi have been used in large number of chemical and electronics applications. Hence the thermal oxidation process is given importance in this study.

Consider the ferromagnetic atom (M) reacting with oxygen as given by equation (3.1)

$$M + O = MO \tag{3.1}$$

This bonding can be explained as ionic based on the fact that M has two valence electrons and O atom has six valence electrons. Based on the density functional calculations on the interaction of the ferromagnetic metal with carbon nanotubes discussed earlier, the two valence electrons are no longer available in 4s level and hence the bonding is less likely to occur. In other words, a longer sustainability is to be expected. Based on this discussion, the thermal oxidation of the ferromagnetic metal should be dependent on the spin polarization. TGA and electrochemical techniques are the ideal tools for studying the oxidation processes. Here we model the TGA behavior based on the interaction.

### 3.1 Model 1

The ferromagnetic metal is considered stable from ambient temperature to a temperature where the thermal oxidation onset occurs as shown in Figure 3.1A. Here the ferromagnetic metal undergoes thermal oxidation at temperature $T_1$. The weight gain occurs due to the oxidative formation of MO. This change in weight is increasing with increasing temperature as expected by Arrhenius equation. When the single ferromagnetic metal is interacting with carbon nanotube and spin polarization occurs, the thermal oxidation would be hindered and the formation of MO and hence the TGA behavior should be modified to the behavior shown in Figure 3.1D. So in a macroscopic system, the polarizer and polarized ones are playing important parts. The amount of polarizer is important.

### 3.2 Model 2

When two ferromagnetic metals are examined by TGA, the two thermal oxidations are distinguishable. Figure 3.1 B shows the thermal oxidations occurring at

two different temperatures $T_1$ and $T_2$. The weight gain associated will be sum of the two oxidation products. Since the onset temperatures are different, the first one onset temperature will show the weight change due to one oxide and upon reaching the second onset temperature both oxides will contribute towards the weight change.

When the two metals are polarized by carbon nanotubes, the TGA behavior will be of that shown in Figure 3.1D indicating that there are no oxides formed.

### 3.3 Model 3

The models developed in the previous sections assumed that the MWCNT is thermally stable throughout the temperature range. If the spin polarizing agent is unstable and undergoes thermal oxidation at a definite temperature far removed from the thermal oxidations of the ferromagnetic metals considered, then at that temperature the ferromagnetic atoms will react with oxygen. This behavior is shown in Figure 3.1C. This case will result in that as shown as shown Figure 3.1weight loss followed by a weight gain.

### 3.4 Model 4

The thermal oxidation features in this situation will depend on the spin polarization of the metals. If there is no spin polarization in both the metals, the alloy should show the thermal oxidative behavior of the first thermal oxidation followed by the second one that is taking place at a higher temperature. It is very similar to Figure 3.1 B. The weight increase will be observed throughout the temperature range after the thermal oxidative onset. In the presence of the MWCNT, which is acting as the spin polarizing agent, the expected behavior will be as shown in Figures 3.1 D.

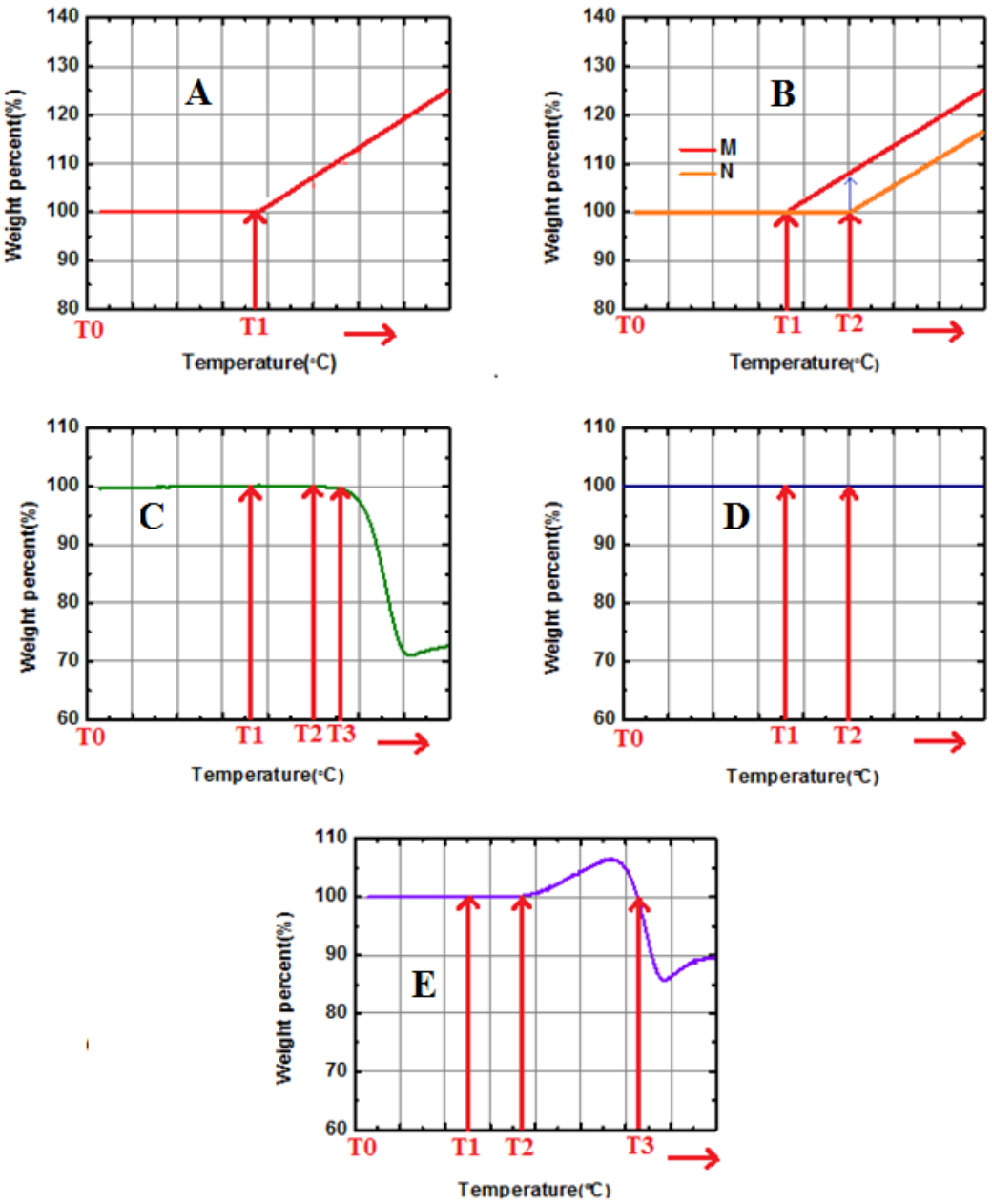


Figure 3.1 Models for spin polarisation

The spin polarization effect can be followed by monitoring the slope dW/dT from the TGA recordings. For a system with no spin polarization, there will be two slopes of zero and positive value. When spin polarization occurs, the positive slope will change to dW/dT=0. If the spin polarizer decomposes, this will not be valid. The data in Chapter 4 gives the measured slopes with different composites.

# CHAPTER 4

With a view to examine the spin polarization of the ferromagnetic atom which will lead to sustainability of the material, the thermogravimetric studies were carried out on atomized cobalt, nickel and cobalt-nickel alloy. The MWCNT is used as the spin polarizing agent.

**4.1 TGA result of Co and MWCNT**

Figure 4.1 shows the TGA of atomized Co from the temperature range of ambient to 800$^{o}$C. The onset of the thermal oxidation is observed at 360$^{o}$C and progresses continuously till 800$^{o}$C in a linear fashion. The weight of the sample increased with temperature indicating that there is a conversion of cobalt to its oxide. Table 4.1 gives the experimental data of the weight gain. The data consistently showed increase in weight up to 800$^{o}$C. When the experiment is performed in nitrogen atmosphere instead of oxygen, no weight change was observed.

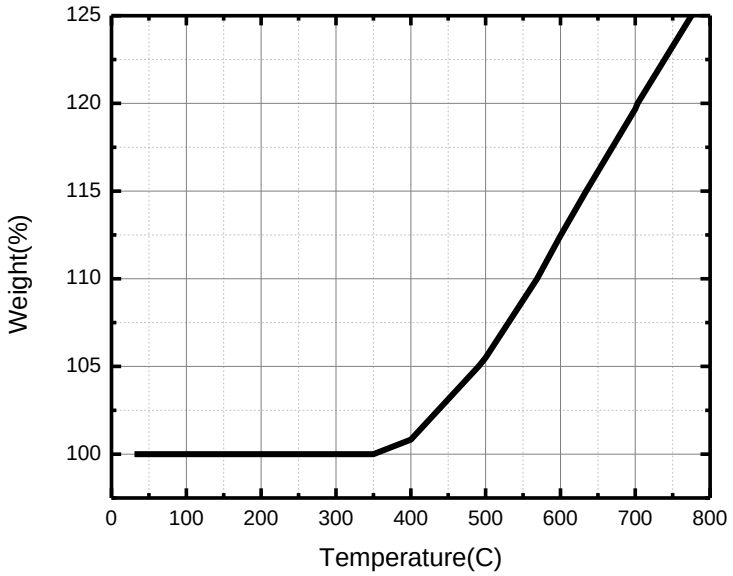


Figure 4.1 TGA of atomized Cobalt in oxygen

Two spin polarizing agents were selected for this work. One was MWCNT and the other was graphite. The TGA behavior of the two carbons was examined. Figure 4.2 shows the TGA of MWCNT in the atmosphere of oxygen. There is no weight change observed from ambient to 600$^{o}$C. Thereafter there was a weight loss observed that steeply changes the curve. At about 750$^{o}$C, the sample in the pan has evaporated leading to a perfect zero weight. This is attributed to the oxidation of the carbon nanotubes to oxides of carbon. The zero weight in the TGA experiment is an indication of no residue being left due to the oxidation process. These results indicate that MWCNT will be a good spin polarizing agent from ambient temperature to 600$^{o}$C. Hence spin polarization can be studied in this temperature range with MWCNT.

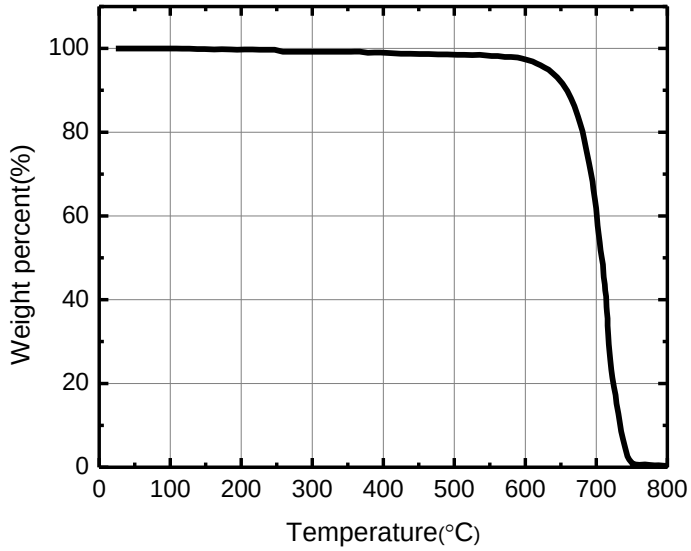


Figure. 4.2 Thermogravimetric curve of MWCNT in air

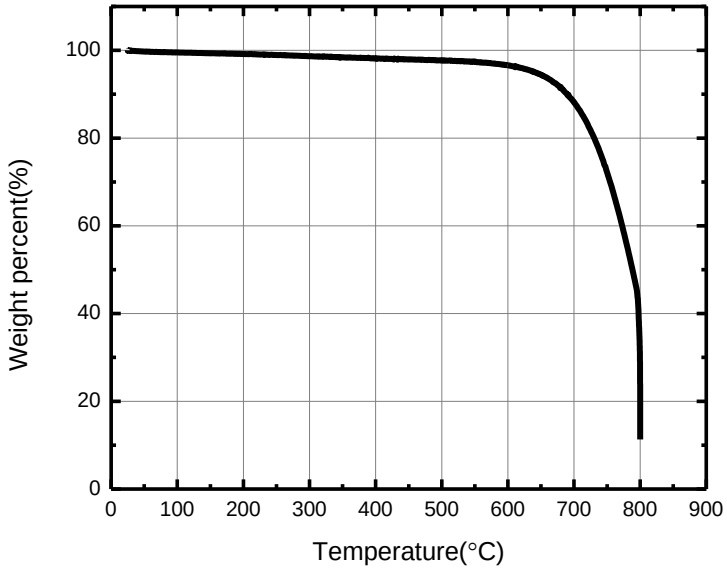


Fig. 4.3 Thermogravimetric curve of graphite in air

**Table 4-1 Weight distribution analysis with atomized cobalt**

| Sample weight (mg) | Weight at 800℃ (mg) | Weight gain (mg) | Weight gain percent (%) | dW%/dT |
|---|---|---|---|---|
| 48.672 | 64.884 | 16.212 | 33.308 | 0,0.0757 |
| 108.46 | 146.258 | 36.798 | 33.928 | 0,0.0771 |

| | | | | |
|---|---|---|---|---|
| 48.354 | 65.245 | 16.891 | 34.932 | 0,0.0794 |
| 64.847 | 86.238 | 21.391 | 32.987 | 0,0.0749 |
| 98.55 | 131.84 | 33.29 | 33.78 | 0,0.0768 |

Figure 4.3 depicts the TGA recording for graphite powder. Unlike the behavior of MWCNT, the weight change starts at about 300$^{o}$C and increases with increasing temperature. At 800$^{o}$C, the weight in the pan reaches a lowest value. Although the behavioral patterns are different, the use of graphite as spin polarising agent is not encouraging although it could be used for comparative studies.

Figure 4.1 demonstrates that atomized Co undergoes thermal oxidation at 360$^{o}$C. When it is composited with MWCNT, it shows the features as shown in Table 4.2.

The TGA results with sintered samples are similar to the unsintered composites. The following figures give the observed features.

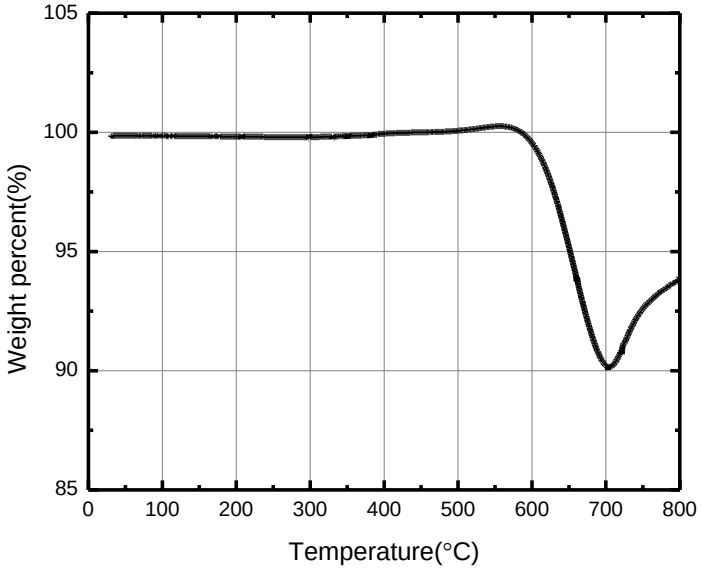


Fig. 4-4 Thermo gravimetric curve of sample Co:MWCNT=4:1 (after sinter 500 ℃ for 30 minutes) in air

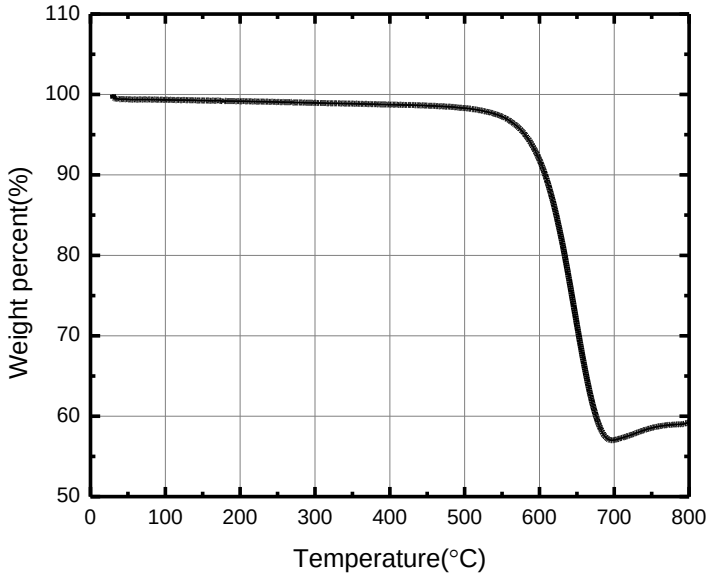


Fig. 4-5 Thermo gravimetric curve of sample Co:MWCNT=1:1 (after sinter 500 ℃ for 30 minutes) in air.

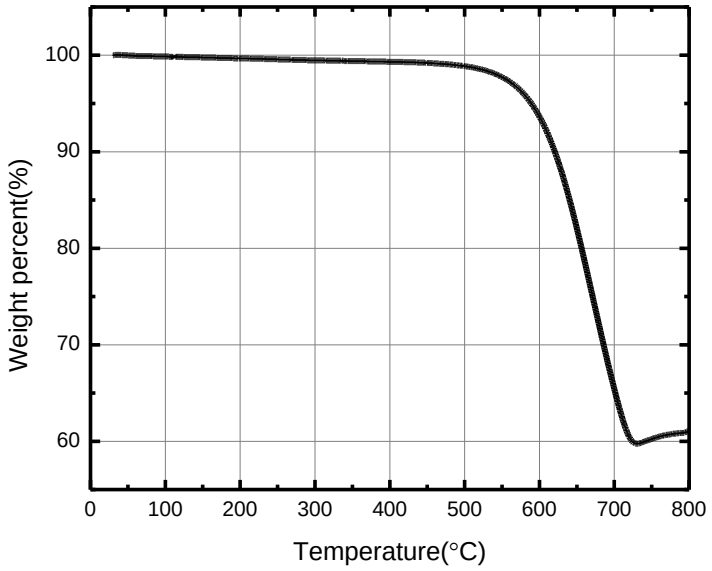


Fig. 4-6 Thermo gravimetric curve of sample Co:MWCNT=1:1 (after sinter 500 ℃ for 60 minutes) in air

Table 4-2 Weight distribution analysis with Co:MWCNT=1:2

| Sample weight(mg) | Weight percent before oxidation (%) | Weight percent after oxidation (%) | dWt%/dT(for the oxidation) | Weight percent at transition (%) |
|---|---|---|---|---|
| 3.301 | 98.55 | 99.89 | 0, 0.011 | 42.28 |

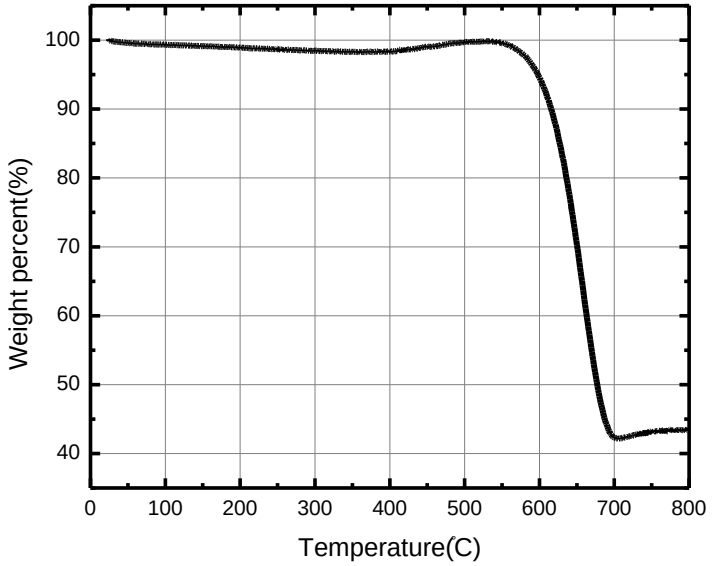


Fig. 4-7 Thermo gravimetric curve of Co:MWCNT=1:2 in air

Table 4-3 Weight distribution analysis with Co:MWCNT=1:1

| Sample weight(mg) | Weight percent before oxidation (%) | Weight percent after oxidation (%) | dWt%/dT(for the oxidation) | Weight percent at transition (%) |
|---|---|---|---|---|
| 3.734 | 98.78 | 98.78 | 0.00 | 58.03 |

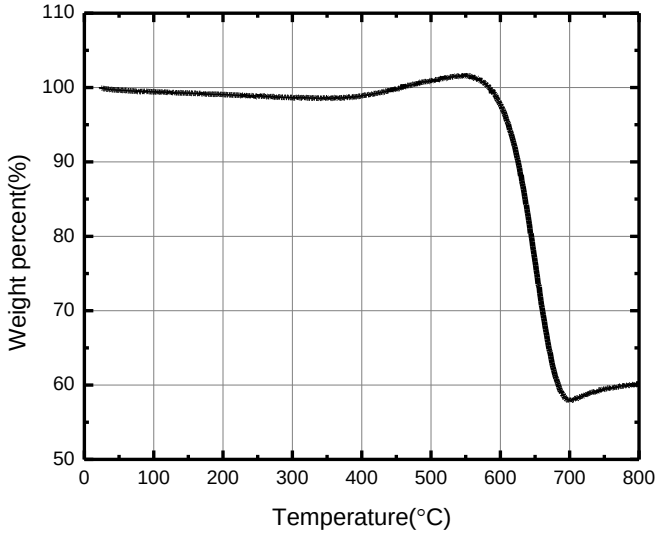


Fig. 4-8 Thermo gravimetric curve of Co:MWCNT=1:1 in air

Table 4-4 Weight distribution analysis with Co:graphite=1:1

| Sample weight(mg) | Weight percent before oxidation (%) | Weight percent after oxidation (%) | dWt%/dT(for the oxidation) | Weight percent at transition (%) |
|---|---|---|---|---|
| 3.301 | 99.20 | 106.3 | 0,0.0244 | 75.4 |

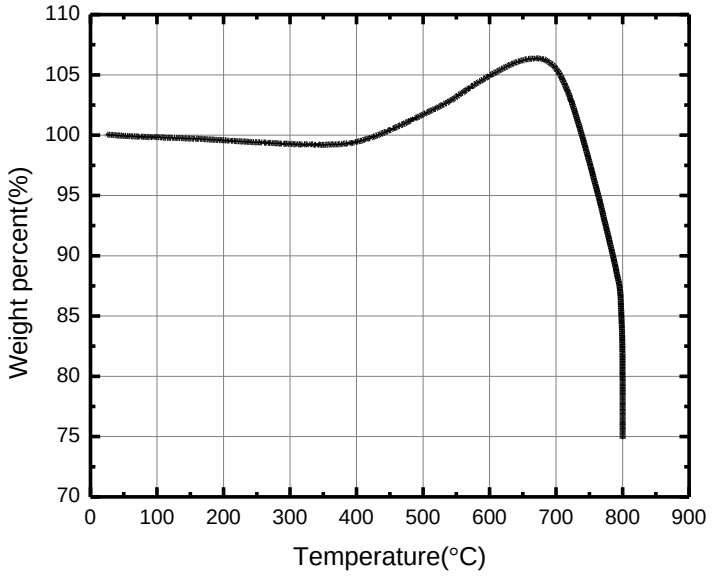


Fig. 4-9 Thermo gravimetric curve of Co:graphite=1:1 in air

Table 4-5 Weight distribution analysis with Co:MWCNT=2:1

| Sample weight(mg) | Weight percent before oxidation (%) | Weight percent after oxidation (%) | dWt%/dT(for the oxidation) | Weight percent at transition (%) |
|---|---|---|---|---|
| 4.63 | 99.29 | 105.6 | 0,0.0309 | 84.85 |

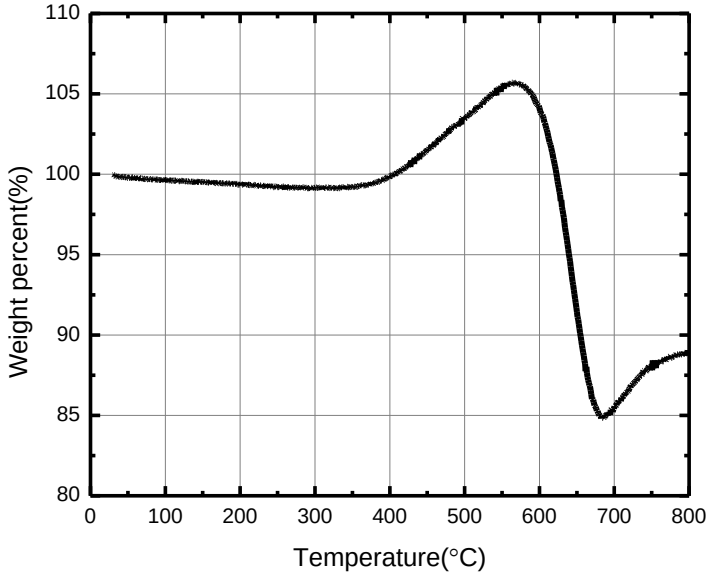


Fig. 4-10 Thermo gravimetric curve of Co:MWCNT=2:1 in air

Table 4-6 Weight distribution analysis with Co:MWCNT=3:1

| Sample weight(mg) | Weight percent before oxidation (%) | Weight percent after oxidation (%) | dWt%/dT(for the oxidation) | Weight percent at transition (%) |
|---|---|---|---|---|
| 5.613 | 99.99 | 106.92 | 0,0.03898 | 94.09 |

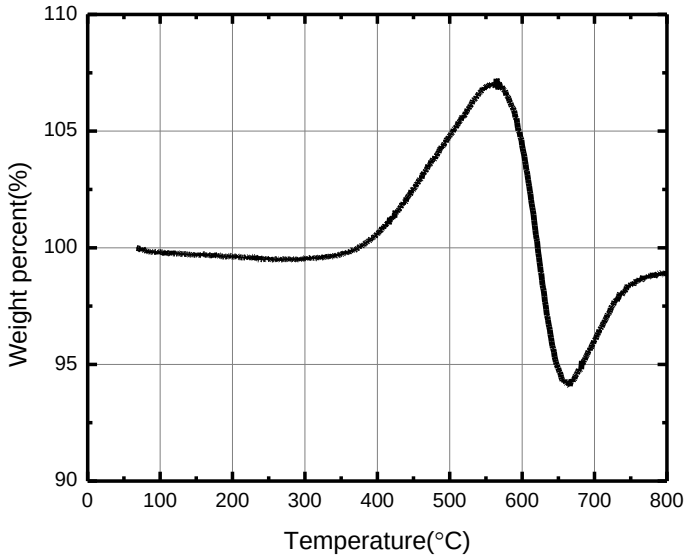


Fig. 4-11 Thermo gravimetric curve of Co:MWCNT=3:1 in air

**4.2 TGA result of Ni and MWCNT**

The atomized Ni showed behavior similar to that of cobalt except the thermal oxidative temperature for Ni is at 500$^{o}$C. Figure 4.12 shows the typical TGA pattern for atomized Ni. When spin polarizing agent is composited with Ni, the TGA pattern changes as shown in Figures 4.13 and 4.14. At the weight ratio of 1:1, the thermal oxidation of Ni is completely absent. However, after the break down of the spin polarizing agent, the ferromagnetic metal is exposed to oxygen along with the decomposition product of MWCNT. Here we observe a weight loss that is more than expected for the system.

The spin polarization effect is felt with the composite of Ni:MWCNT in the weight ratio of 1:1. At this weight ratio, there is only one slope of dW/dT=0 until the break down of MWCNT is observed.

At a temperature of 800$^{o}$C, the weight analysis shows that there is a loss of nickel. Tables 4.1 and 4.2 give the deviations observed between Co and Ni composites. There is a loss of material that is attributed to the formation of nickel tetracarbonyl. It has boiling point of 45$^{o}$C. In contrast Co is known to be inert to reacting with carbon monoxide and does not form the carbonyl. This difference in behavior is shown in the Tables 4.1 and 4.2.

**Table 4-7 TGA Data At 800° C for Cobalt Composite**

| System[1] | TGA Weight at 800 C, mg | Original weight, mg | | Difference[2], mg | Gain[3], mg |
|---|---|---|---|---|---|
| | | Co | MWCNT | | |
| Co:MWCNT(1:1) | 1.518 | 1.241 | 1.241 | 0.964 | 0.277 |
| Co:MWCNT(1:1) | 1.865 | 1.418 | 1.418 | 0.971 | 0.447 |
| Co:MWCNT(4:1) | 4.675 | 3.982 | 0.995 | 0.302 | 3.680 |

1. Sintered sample at 500 C
2. Difference=[Original weight of the sample in the pan – Weight of the sample at 800 C]
3. Gain=[Weight of the sample at 800 C – original weight of Co in the composite]

**Table 4-8 TGA Data At 800 C for Nickel Composite**

| System[1] | TGA Weight at 800 C, mg | Original weight, mg | | Difference[2], mg | Gain[3], mg |
|---|---|---|---|---|---|
| | | Ni | MWCNT | | |
| Ni:MWCNT(1:1) | 1.0249 | 1.352 | 1.352 | 1.679 | -0.327 |
| Ni:MWCNT(1:1) | 0.3110 | 0.778 | 0.778 | 1.245 | -0.467 |
| Ni:MWCNT(4:1) | 0.9854 | 2.066 | 0.516 | 1.597 | -0.469 |

1. Sintered sample at 500 C
2. Difference=[Original weight of the sample in the pan – Weight of the sample at 800 C]
3. Gain=[Weight of the sample at 800 C – original weight of Ni in the composite]

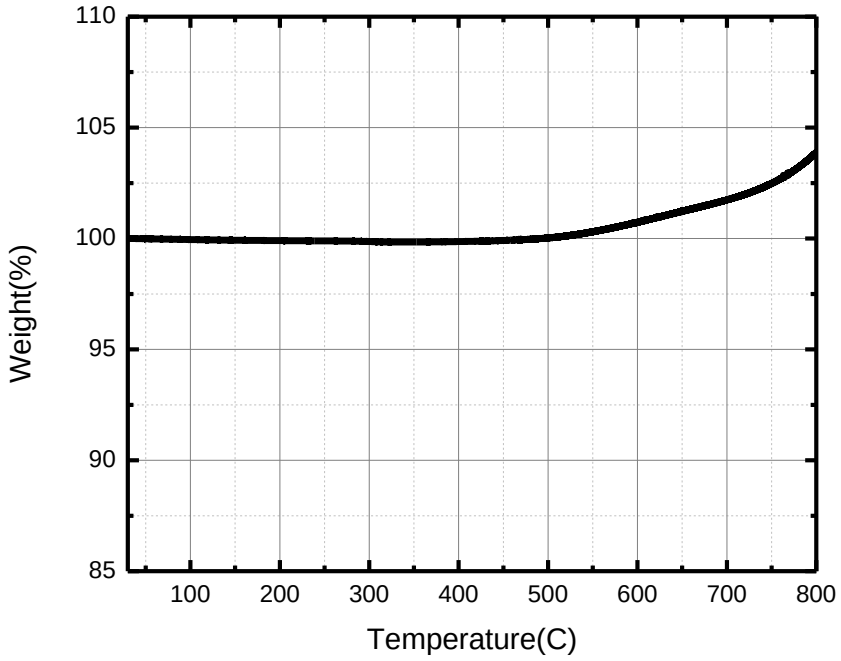


Fig. 4-12 Thermo gravimetric curve of atomized Nickel in air

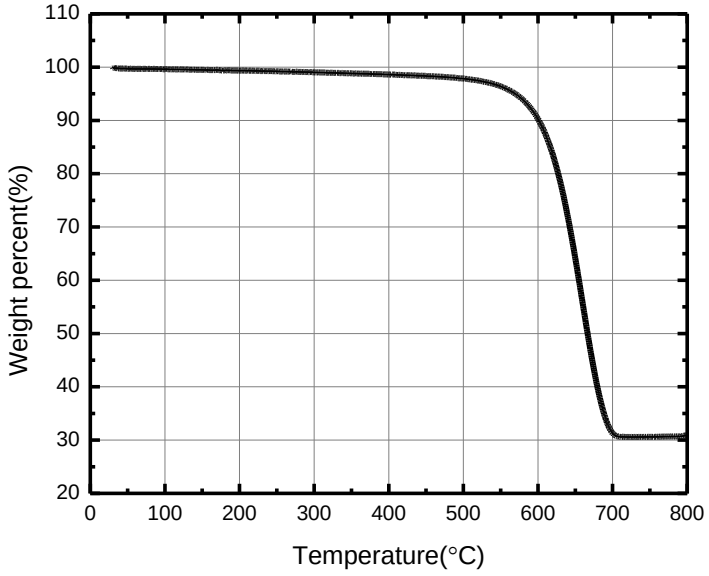


Fig. 4-13 Thermo gravimetric curve of sample Ni:MWCNT=4:1 (after sinter 500℃ for 30 minutes) in air

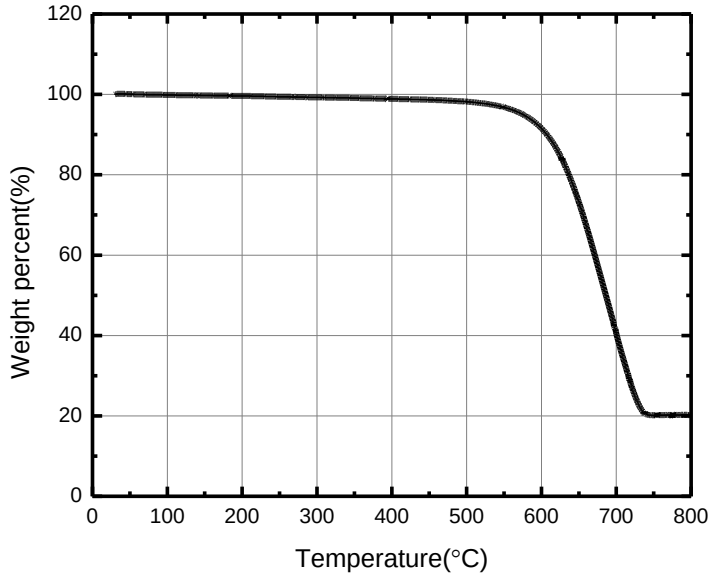


Fig. 4-14 Thermo gravimetric curve of sample Ni:MWCNT=1:1 (after sinter 500℃ for 30 minutes) in air

**4.3 TGA result of CoNi alloy**

The TGA of CoNi (1:1) is shown in Figure 4.15. The thermal oxidation of the alloy starts at 500$^{o}$C. This temperature corresponds to the thermal oxidation of atomized Ni. There is no thermal oxidation of Co observed. The components present in the alloy were examined by XRD which gave 2 theta reflections corresponding to Co at 66.7$^{o}$ and 77.5$^{o}$ and Ni at 57.9$^{o}$ and 61.7$^{o.}$ (Figure 4.31).

In Figure 4.15 two distinct slopes are visible that is arising from the thermal oxidation of the alloy. In the presence of spin polarizing agent, there is only one slope of zero as shown in the figure. The following figures (Figures 4.15-4.26) represent attempts at understanding the behavior of CoNi interaction with MWCNT of different ratios. Here again in a large number of experiments, the weight ratio of alloy to MWCNT of 1:1 provided complete polarization. Transforming the weight ratio to atomic ratio of the alloy to carbon of 5 is obtained. It indicates that five carbon atoms are surrounding the alloy in protecting it from the thermal oxidation.

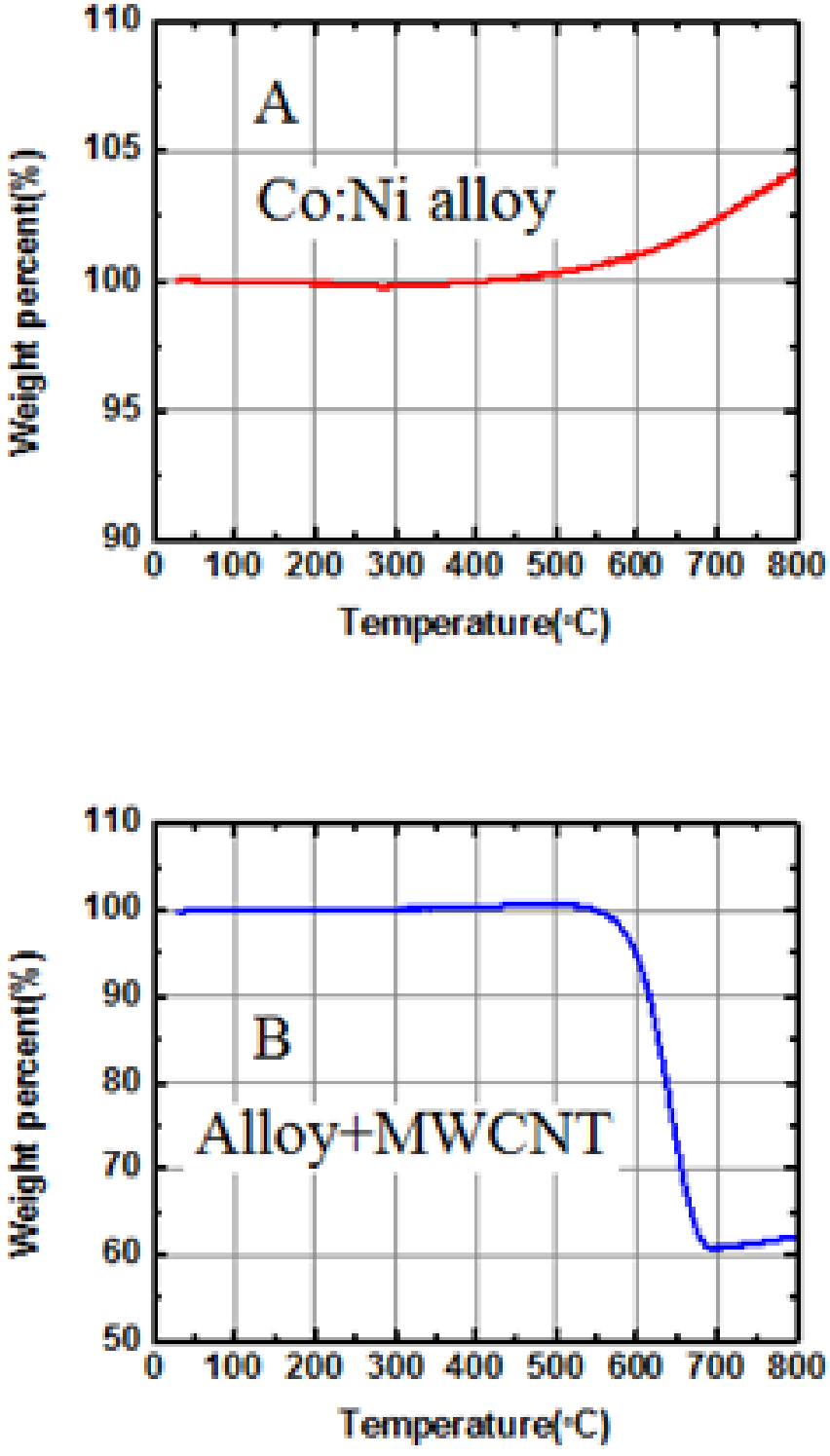


Figure 4.15 TGA of CoNi alloy and alloy in the presence of MWCNT (1:1)

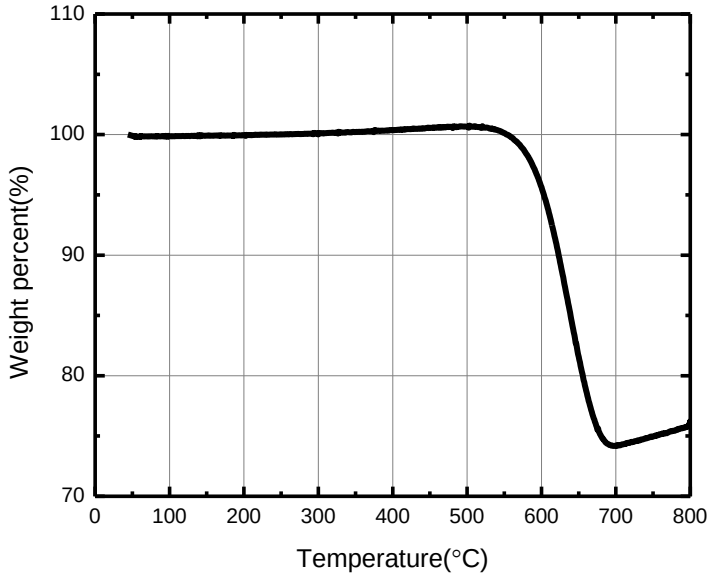


Fig. 4-16 Thermo gravimetric curve of (CoNi=1:1alloy):MWCNT=3:1 in air

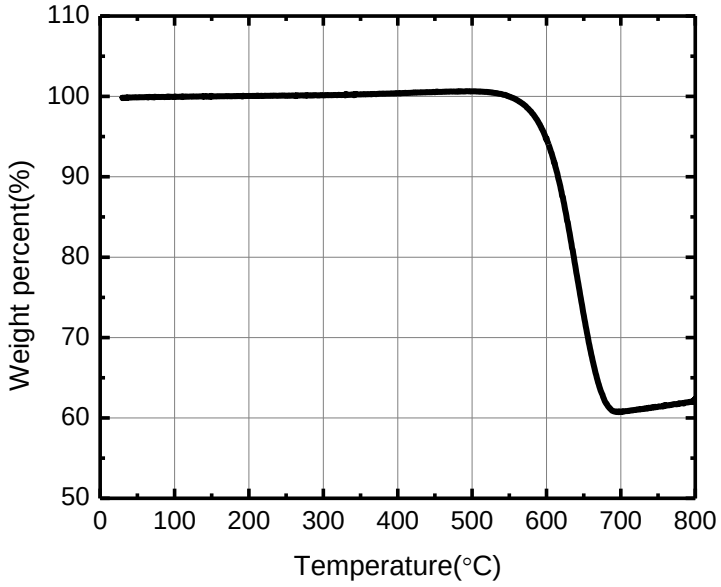


Fig. 4-17 Thermo gravimetric curve of (CoNi=1:1alloy):MWCNT=2:1 in air

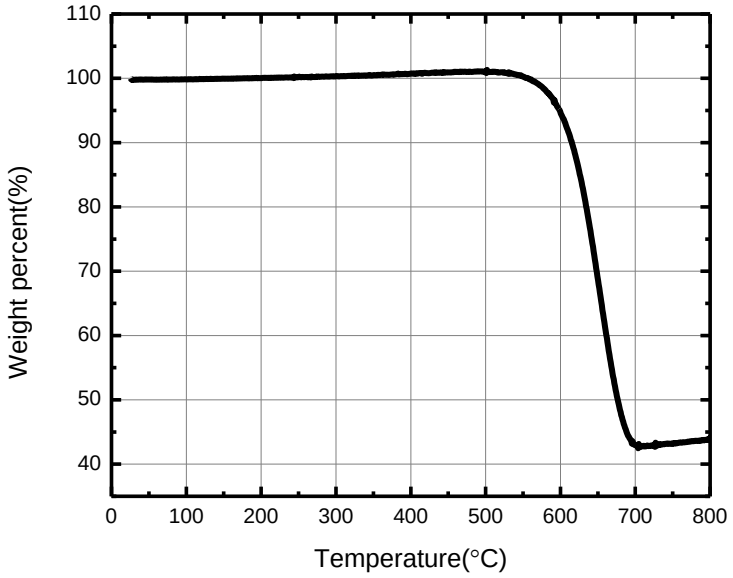


Fig. 4-18 Thermo gravimetric curve of (CoNi=1:1alloy):MWCNT=1:1 in air

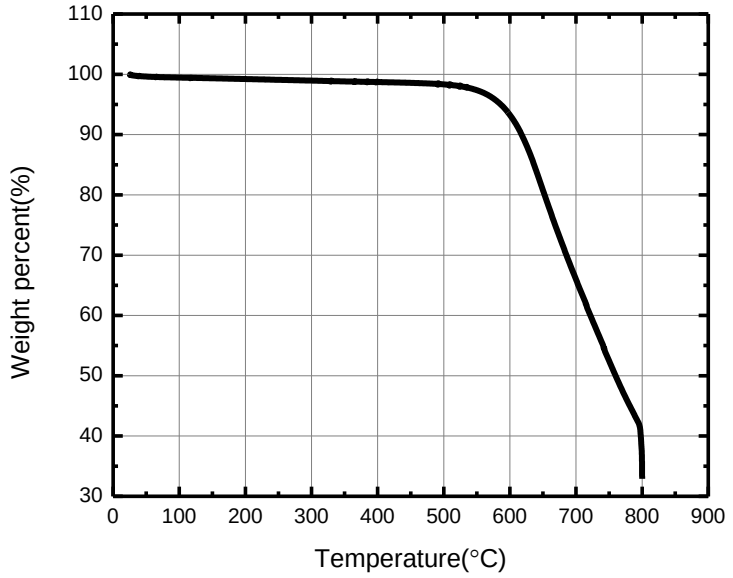


Fig. 4-19 Thermo gravimetric curve of (CoNi=1:1alloy):MWCNT=1:2 in air

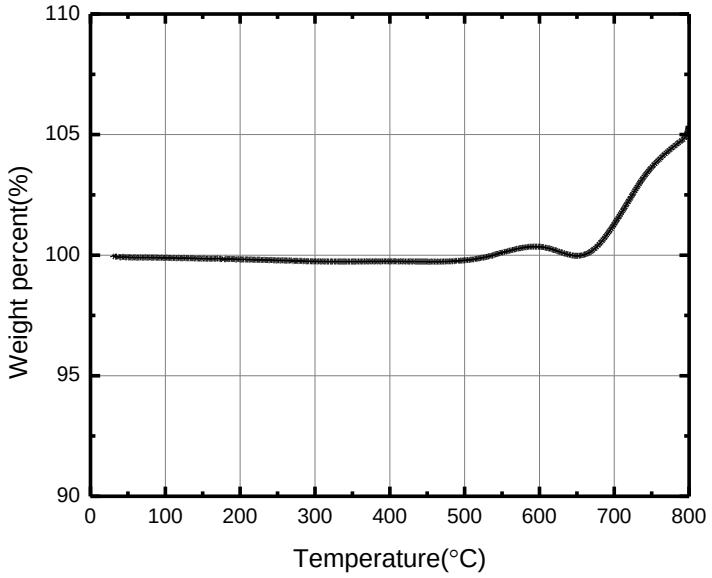


Fig. 4-20 Thermo gravimetric curve of Co:Ni:MWCNT=1:1:0.1 (sinter 500 ℃ for 30 minutes) in air

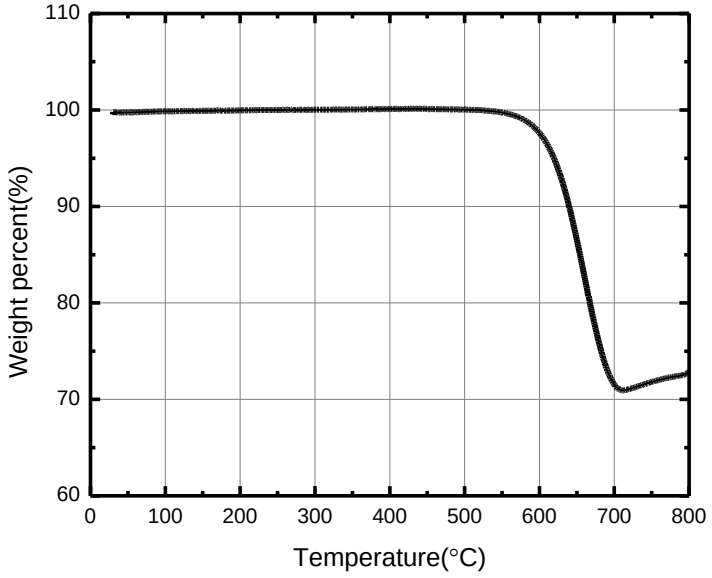


Fig. 4-21 Thermo gravimetric curve of Co:Ni:MWCNT=1:1:1 (sinter 500 ℃ for 30 minutes) in air

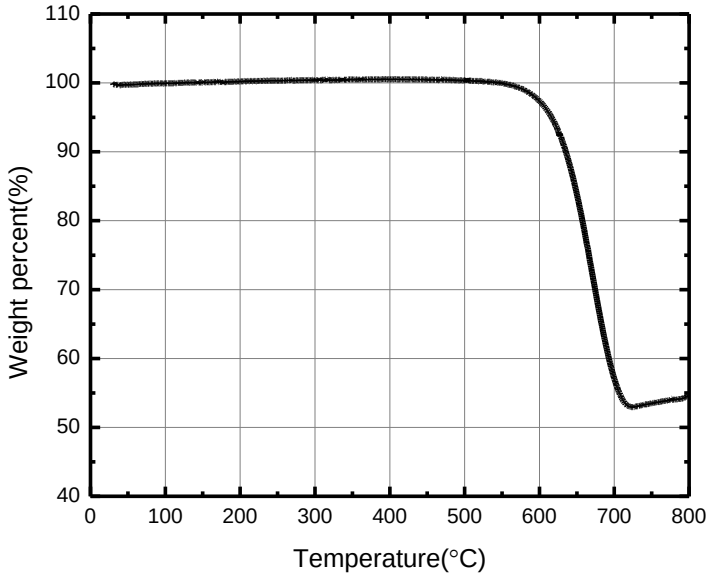


Fig. 4-22 Thermo gravimetric curve of Co:Ni:MWCNT=1:1:2 (sinter 500℃for 30 minutes) in air

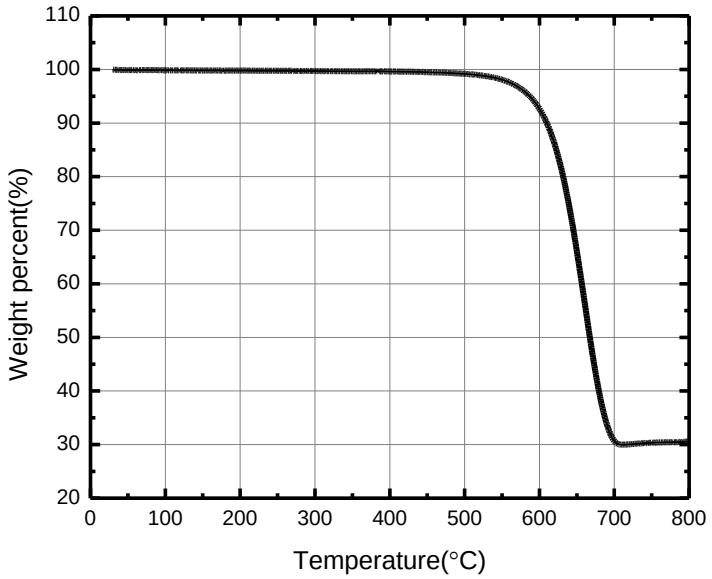


Fig. 4-23 Thermo gravimetric curve of CoNi:MWCNT=1:1:4 (sinter 500℃for 30 minutes) in air

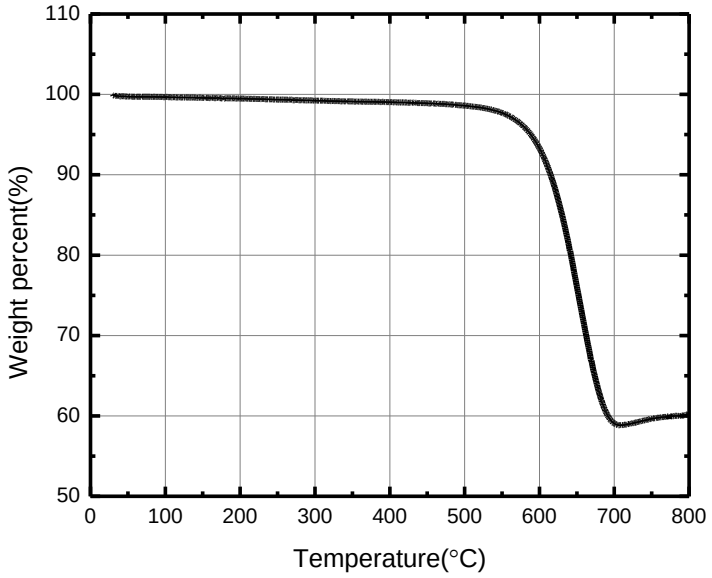


Fig. 4-24 Thermo gravimetric curve of Co:Ni:MWCNT=1:1:1( sinter 500℃ for 1 hour) in air

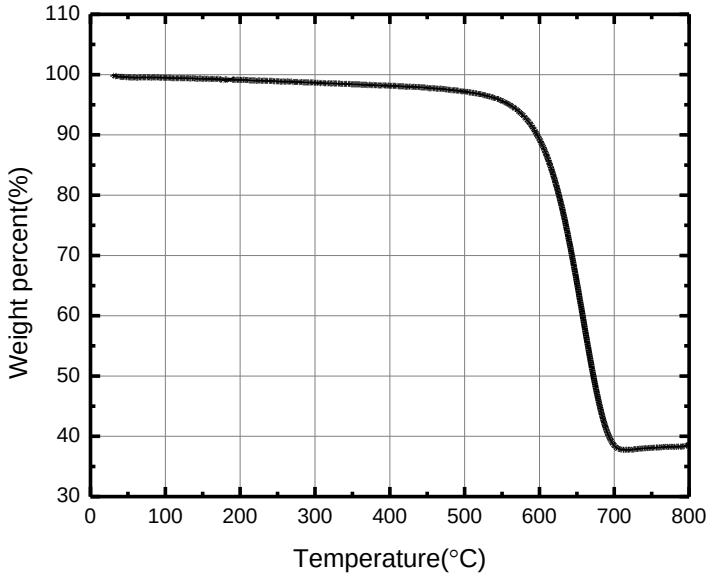


Fig. 4-25 Thermo gravimetric curve of Co:Ni:MWCNT=1:1:2 ( sinter 500℃ for 1 hour) in air

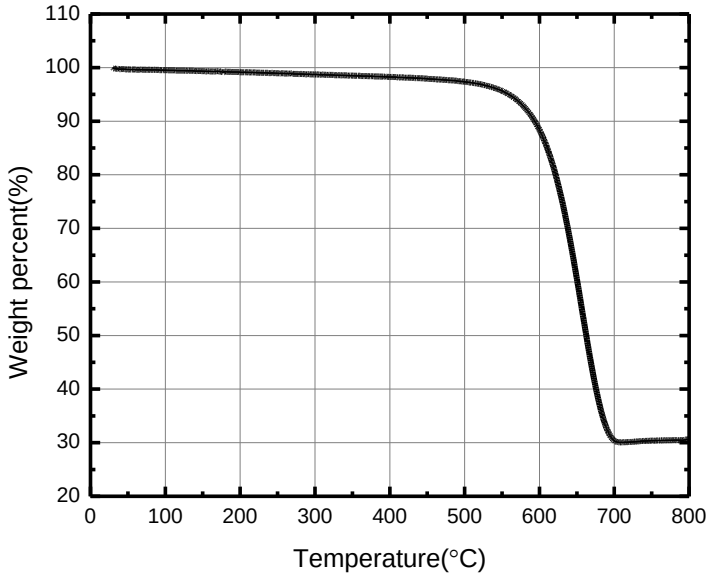


Fig. 4-26 Thermo gravimetric curve of CoNi:MWCNT=1:1:4 ( sinter 500℃ for 1 hour) in air

**4.4 FTIR results and discussion**

The thermal oxidation products have been examined by FTIR measurements. Figure 4-27 shows the alloy alone and in the presence of MWCNT. The alloy shows peaks at 595 $cm^{-1}$ and 660 $cm^{-1}$. These peaks are absent when composited with MWCNT.

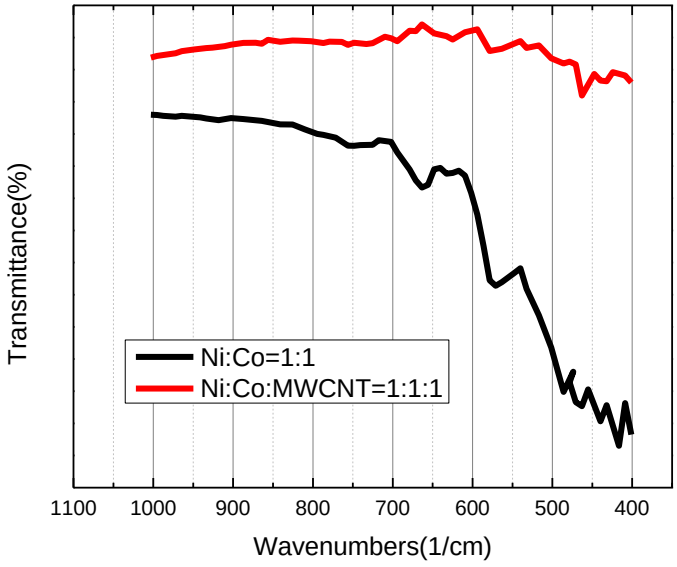


Fig. 4-27 FTIR of the alloy alone and in the presence of spin polarizer

# CHAPTER 5

The sustainability of CoNi has been of great interest in several practical applications such as in energy storage systems, catalysis and related fields. In this chapter we examine the sustainability of CoNi composited with MWCNT behavior using Tafel measurements.

## 5.1 Tafel plot results and discussions

The experiments were carried out in aqueous medium using the composited alloy with MWCNT with atomic ratio of 16.9:83.10 (corresponding to weight ratio of 1:1). This material showed the ideal polarizing conditions in TGA. The initial potential is set at -0.50 V and a scan rate of 1 mV/s. The final potential is set at 0.50V. The open circuit potential is measured as -0.2475V. Figures 5.1 to 5.4 show the Tafel curves obtained in different electrolytes. In these curves, on the anodic part, there is a small peak appears due to desorption of hydrogen. The corrosion current density is evaluated from the Tafel plots and an average value of 4.29 X $10^{-8}$A/cm$^2$ has been obtained. Table 5.1 gives the performance of CoNi and the composite. The stability of platinum was measured in the above electrolytes in Figures 5.5-5.7 by recording Tafel curves.

**Table 5.1 Relative performance of Corrosion rates**

| Material | Corrosion Current Density, A/cm$^2$ | Open circuit Potential,V | Corrosion Rate, gmd |
|---|---|---|---|
| CoNi[75] | 3.5 X$10^{-4}$ | -0.499 | 91.8 |
| CoNi:MWCNT | 1.0 X$10^{-6}$ | -0.2475 | 0.26 |
| Pt | 4.29 X$10^{-8}$ | 0.1580 | 0.01 |

gmd:gram/squaremeter.day

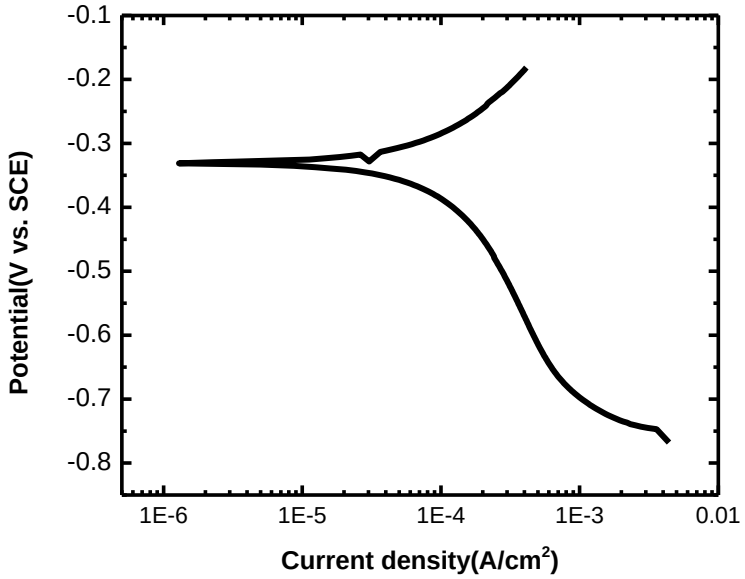


Fig.5-1Polarization Tafel scans of Ni:Co:MWCNT=1:1:1(sinter 500℃ for 2 hours) in 0.2M potassium chloride

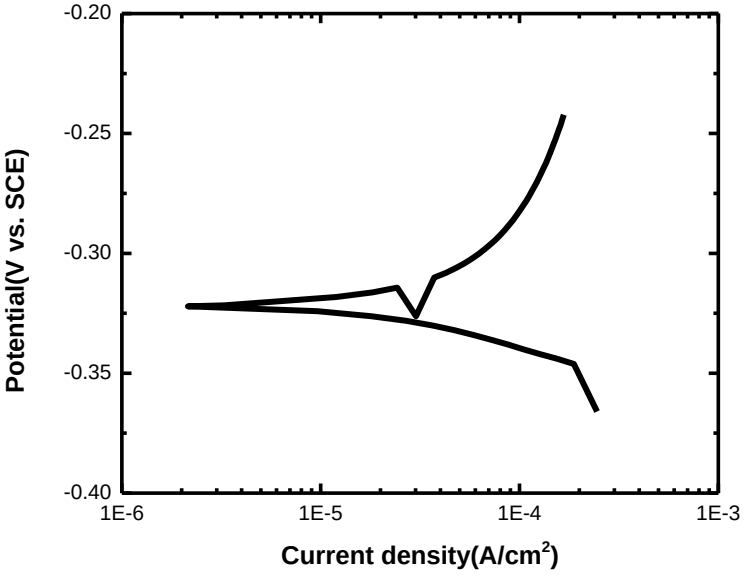


Fig.5-2 Polarization Tafel scans of Ni:Co:MWCNT=1:1:1(sinter 500℃ for 2 hours) in 0.2M sodium sulfate

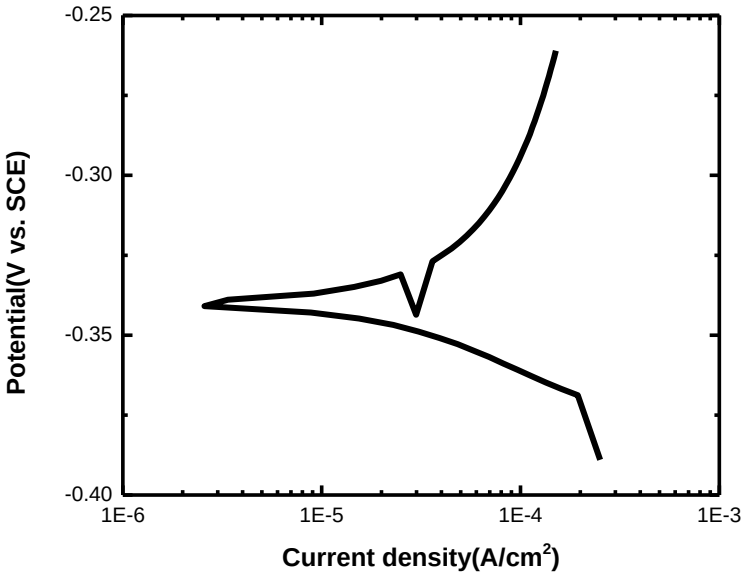


Fig.5-3 Polarization Tafel scans of Ni:Co:MWCNT=1:1:1(sinter 500℃ for 2 hours) in 0.2M sodium sulfate (Duplicate experiment)

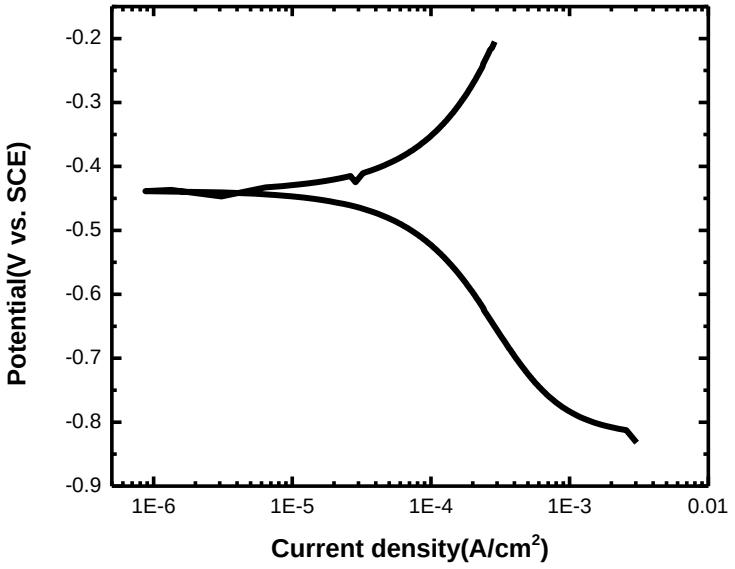


Fig.5-4 Polarization Tafel scans of Ni:Co:MWCNT=1:1:1(sinter 500℃ for 2 hours) in 0.2M sodium sulfate (Duplicate experiment)

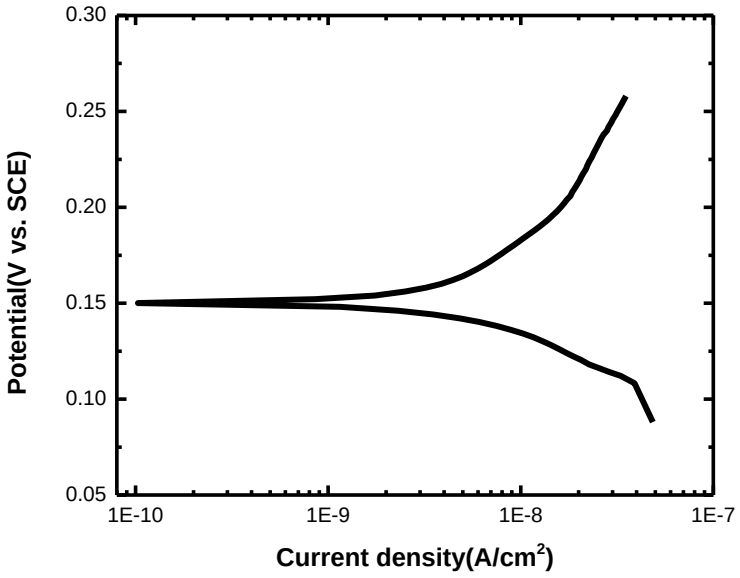


Fig.5-5 Polarization Tafel scans of platinum disc in 0.2M sodium sulfate

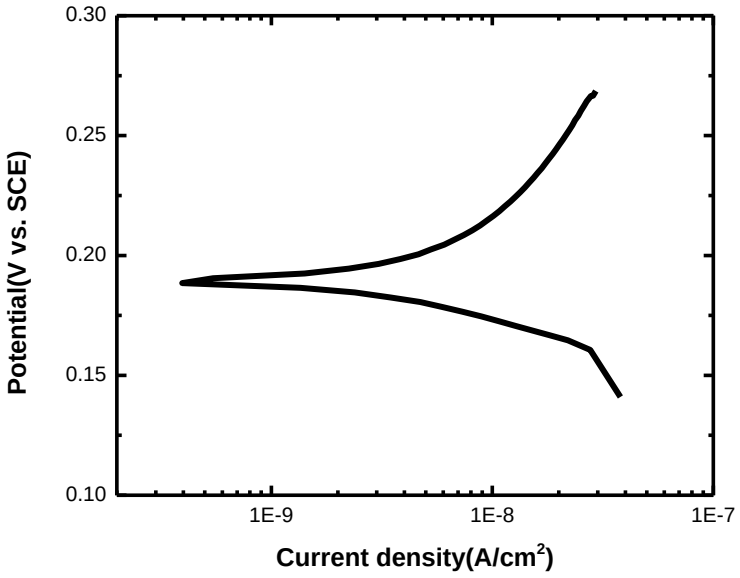


Fig.5-6 Polarization Tafel scans of platinum disc in 0.2M sodium sulfate (Duplicate Experiment)

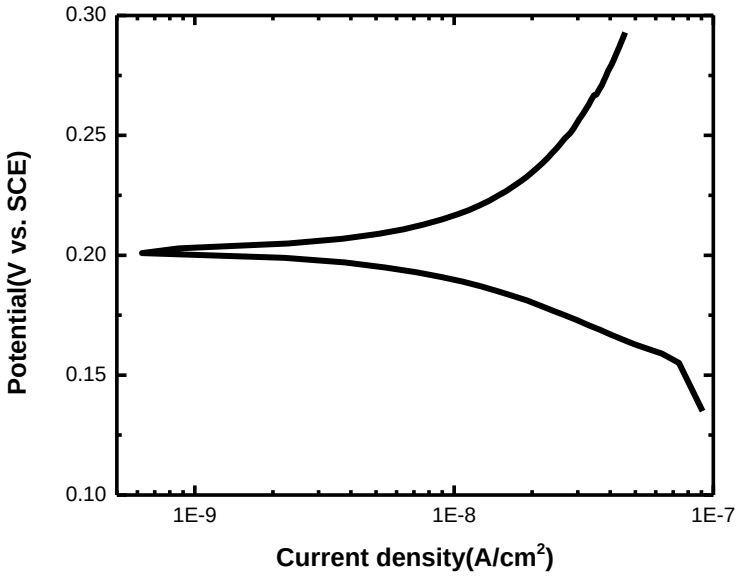


Fig.5-7 Polarization Tafel scans of platinum disc in 0.2M sodium sulfate

**5.2 Current-Voltage curves**

The current voltage curves at the alloy electrode are remarkably catalytic as shown by Figures 5-8 through 5-10. Table 5.2 gives the data for the magnitude of currents flowing.

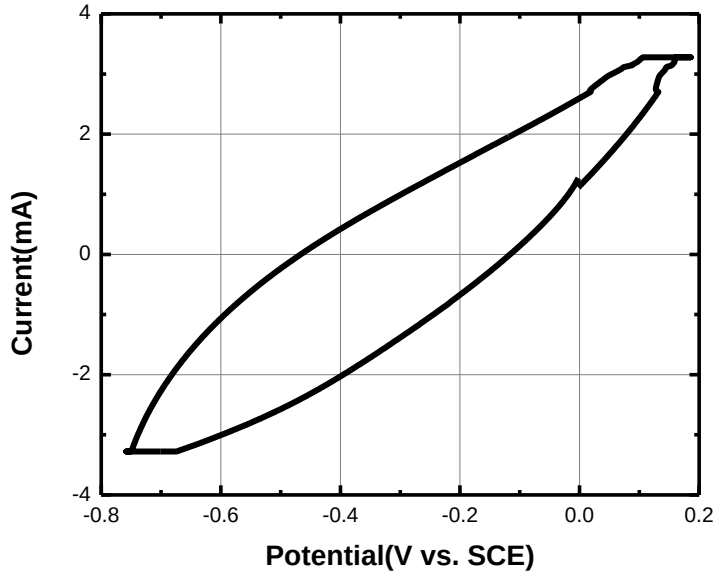


Fig.5-8 Cyclic voltammetry of Ni:Co:MWCNT=1:1:1(sinter 500℃ for 2 hours) in 0.2M potassium chloride

Table 5.2 CV potential and current

| Intermediate | Electrode materials | E (V) | ia(A/cm2) | ic(A/cm2) |
|---|---|---|---|---|
| $Na_2SO_4$ | Pt | 0 | 7.16E-5 | 3.92E-5 |
| $Na_2SO_4$ | Pt | -0.5 | 1.08E-5 | 1.08E-5 |
| $Na_2SO_4$ | Pt | 0.5 | 8.11E-7 | 5.54E-5 |
| $Na_2SO_4$ | CoNi:MWCNT=1:1:1 | 0 | 0.045 | -7.57E-3 |
| $Na_2SO_4$ | CoNi:MWCNT=1:1:1 | -0.5 | 0.014 | -0.038 |
| $Na_2SO_4$ | CoNi:MWCNT=1:1:1 | 0.5 | 0.066 | 0.0423 |

$i_a$ : Anodic current; $i_c$: cathodic current

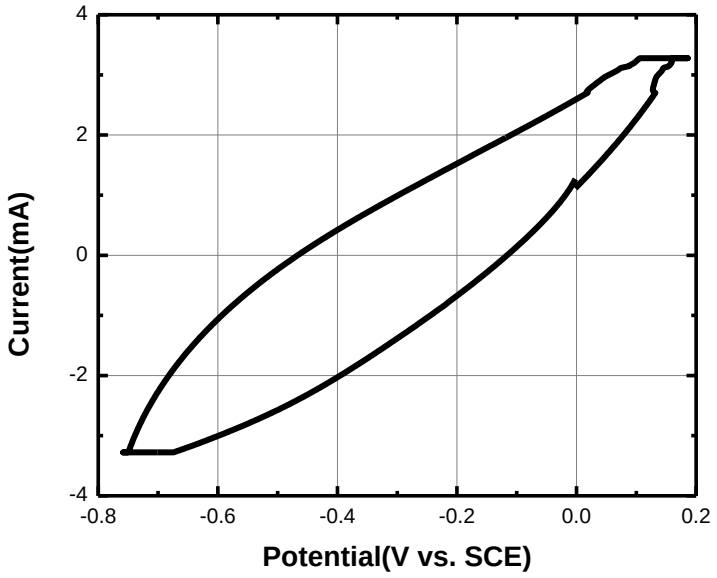


Fig.5-9 Cyclic voltammetry of Ni:Co:MWCNT=1:1:1(sinter 500℃ for 2 hours) in 0.2M sodium sulfate

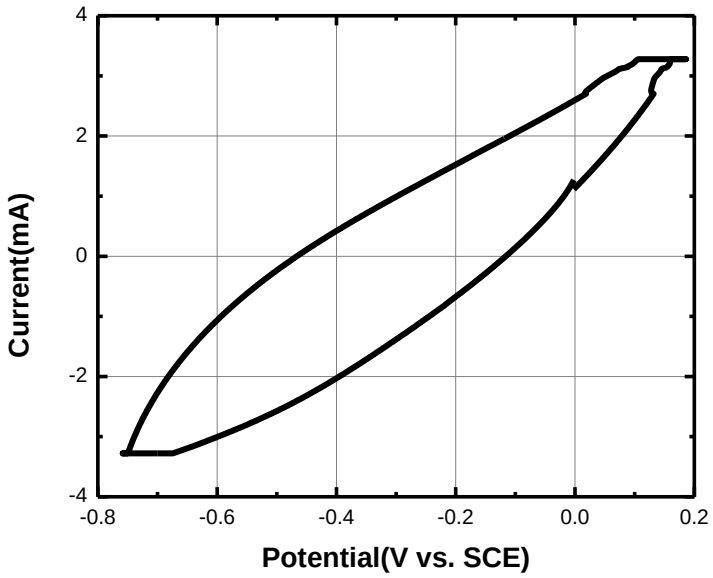


Fig.5-10 Cyclic voltammetry of platinum disc in 0.2M sodium sulfate

# CHAPTER 6

## 6 Conclusions

The results obtained with ferromagnetic metals in atomized state interact with MWCNT. The interaction changes the electronic configuration by a transition of 4s electrons moving to 3d level making the metal inert to thermal oxidation. This carbon nanotube interaction has been followed by TGA measurements. There are two slopes observed in TGA with the atomized ferromagnetic metal or its alloy (CoNi). The first slope is zero and the second one has a positive value. The positive value decreases with the interaction of MWCNT and reaches a value of zero when the interaction is complete. Table 6.1 gives the composition data.

**Table 6.1 Optimization**

| Ferromagnetic metal, M | Ratio (MWCNT/M) | dW/dT μg/$^{o}$C |
|---|---|---|
| Co | 0 | 0, 39.0 |
| Co:MWCNT | 5 | 0 |
| Co:MWCNT | 1.22 | 0, 11.0 |
| Ni | 0 | 0,37.0 |
| Ni:MWCNT | 5 | 0 |
| Ni:MWCNT | 1.22 | 0,4.0 |
| CoNi | 0 | 0,5.7 |
| CoNi:MWCNT | 3.2 | 0,3.8 |
| CoNi:MWCNT | 5 | 0,0 |

On the basis of this optimization data, it appears that the ferromagnetic atom is surrounded by five carbon atoms for complete spin polarization.

The Ni composite tends to form a volatile complex at 800$^{o}$C in the TGA measurements, that is absent with the cobalt composite. As a result, the weight changes observed at 800$^{o}$C are lower than would be predicted with the nickel composites.

The sustainability of CoNi alloy has been examined by Tafel analysis. The results obtained show that the composited alloy with MWCNT has a corrosion rate of

0.26 gmd which is about 350 times slower than the uncomposited material. The measured open circuit voltages are in concurrence with the trend observed.

### 6.1 Future work

Based on the results reported in this thesis, it is important to carry out further work on detailed XRD characterization of the composited materials during different stages of TGA measurements that will give insight into the mechanism. In particular the Ni composites show interesting behavior of gaseous compound formation that could be characterized by using mass spectral information. The CoNi alloy is interesting in that the spin polarization of Co can be examined by ESCA and XPS. On the sustainability measurements, the study of these systems by electrochemical impedance spectroscopy will give more details on the mechanism of stabilization.

**References**


[1] P. Dubey, D. Muthukumaran, S. Dash, R. Mukhopadhyay and S. Sarkar, Pramana, 65, 687-97(2005) .

[2] H.S.Philip Wong and Deji Akinwande (2011). Carbon Nanotube and Graphene Device Physics. New York, NY: Cambridge University Press

[3] L.V.Radushkevich and V.M. Lukyanovich. Zh. Fis. Khim. (Russ.J.Phys.Chem.).26,88-95 (1952).

[4] W.R.Davis, R.J.Slawson and G.R.Rigby, Nature, 171, 756 (1953).

[5] L.J.E.Hofer, E.Sterling and J.T.McCartney. J.Phys.Chem., 59, 1153-5 (1955).

[6] Chih-Kai Yang, Jijun Zhao, and Jian Ping Lu, Physical Review 90, 25(2003)

[7] G.A. Prinz, Science 282, 1660(1998).

[8] S.A. Wolf , Science 294, 1488(2001)

[9] M.S. Dresselhaus, G. Dresselhaus, and P. Avouris, Springer-Verlag, Berlin, Germany, 2001.

[10] R.H. Baughman, A.A. Zakhidov, and W.A. de Heer, Science 297, 787(2002).

[11] K. Tsukagoshi, B.W. Alphenaar, and H. Ago, Nature(London) 401, 572(1999).

[12] M.Julliere, Phys, Lett. 54A, 225(1975).

[13] R.Meservey and P.M. Tedrow, Phys. Rep. 238, 173(1994).

[14] L.Balents and R. Egger, Phys. Rev. Lett. 85, 3464(2000); Phys. Rev. B 64, 035310(2001); Q.Si, Phys. Rev. Lett, 81, 3191(1998).

[15] H. Mehrez, J. Taylor, H. Guo, J. Wang, and C. Roland, Phys. Rev. Lett. 84, 2682(2000).

[16] A. Szafer and A.D.Stone, Phys. Rev. Lett. 62, 300(1989).

[17] S. Datta, Electronic Transport in Mesoscopic Systems (Cambridge University Press, Cambridge, UK., 1995).

[18] For a recent review of filling single-wall carbon nanotubes, see M. Monthioux, Carbon 40, 1809 (2002).

[19] C. Guerret-Piécourt, Y. Le Bouar, A. Loiseau, and H. Pascard, Nature (London) 372, 761 (1994).

[20] L. C. Qin, J. Mater. Sci. Lett. 16, 457(1997).

[21] S. Seraphin, D. Zhou, and J. Jiao, J. Appl. Phys. 80, 2097 (1996).

[22] A. Chu, Chem. Mater. 8, 2751 (1996).

[23] J. Sloan et al., Chem. Commun. No. 13, 1319 (2002), and references therein.

[24] Y. Zhang and H. Dai, Appl. Phys. Lett. 77, 3015 (2000).

[25] Y. Zhang, N. W. Franklin, R. J. Chen, and H. Dai, Chem. Phys. Lett. 331, 35 (2000).

[26] C.K.Yang, J.Zhao, and J.P.Lu, Physical Review B 66, 041403 (2000).

[27] N. Rawat, R. Gudyaka, M. Kumar, B. Joshi, and K.S.V.Santhanam, Journal of Nanoscience and Nanotechnology, Vol. 8, 2044-2048, 2008.

[28] B. Joshi, S. Gupta, N. Kalra, R. Gudyaka, and K. S. V. Santhanam, Journal of Nanoscience and Nanotechnology, Vol. 10, 1-6, 2010.

[29] B.S. Fagan and R. Mota, Phys. Rev. B 67, 205414(2003)

[30] S. Iijima, Nature 354, 56 (1991).

[31] K.S.V.Santhanam, R. Sangoi, and L. Fuller, Sens. Actuators B 106, 766(2005).

[32] Y.D.Zhao, W.D.Zhang, H.Chen, and Q.M.Luo, Sens. Actuators B 92, 279(2003).

[33] D.R.Kauffman and A. Star, Angerwandtechemie-International Edition 47, 6550(2008).

[34] T.Zhang, S.Mubeen, N.V.Myung, and M.A.Deshusses, Nanotechnology 19, 332001(2008).

[35] J.C.Ndamanisha and L.P.Guo, Biosens. Bioelectron. 23, 1680(2008).

[36] D.W.Hatchett and M.Josowicz, Chem. Rev. 108, 746(2008).

[37] H.C.Wang, Y.Li, and M.J.Yang, Sens. Actuators B-Chem. 24, 360(2007).

[38] B.Zhao, R.W.Fu, M.Q.Zhang, W.Zeng,M.Z.Rong, and Q.Zheng, J.Mater.Sci.42,4575(2007).

[39] Y.S.Chen, Y.Li, H.C, and H.C.Wang, Carbon 45,357(2007).

[40] X.J.Huang, H.S.Im, and O.Yarimaga, J.Phys. Chem. B 110, 21850(2006).

[41] W.Xue and T.H.Cui, Sensor Letters 6, 675(2008).

[42] M.McGrath and A.V.H.Pham, Sensor Letters 6,719(2008).

[43] R.T.Kachoosangi, M.M.Musameh, I. Abu-Yousef, J.M.Yousef, S.M.Kanan, L.Xiao, S.G.Davies, A.Russell, and R.G.Compton, Anal. Chem 8, 442(2009).

[44] S.Y.Niu, M.Zhao, L.Z.Hu, and S.W.S.Zhang, Sens. Actuators B 135, 200 (2008).

[45] K.Lee, J.W.Lee, K.Y.Dong, and B.K.Ju, Sens. Actuators B 135, 214(2008).

[46] I.Sayago, H.Santos, M.C.Horrillo, M.Aleixandre, M.J.Fernandez, E.Terrado, I.Tacchini I, R.Aroz, W.K.Maser, A.M.Benito, M.T.Martinez, J.Gutierrez, and

E.Munoz, Talanta 77, 758(2008).

[47] H.Richter, M.Treska, J.B.Howard, J.Z.Wen, S.B.Thomasson, A.A.Reading, P.M.Jardim, and J.B.Vander Sande, J.Nanosci. Nanotechnol.8, 6065(2008).

[48] J.R.Wood, Q.Zhao, M.D.Frogley, E.R.Meurs, A.D.Prins, T.Peijs, D.J.Dunstan, and H.D.Wagner, Phys. Rev. B 62, 7571(2000).

[49] H.T.Ng, A.P.Fang, J.Li, and S.F.Y.Li, J.Nanosci. Nanotechnol. 1, 375(2001).

[50] Y.Wang, C.A.Di, Y.Q.Liu, H.Kajiura, S.H.Ye, L.C.Cao, D.C.Wei, H.L.Zhang, Y.M.Li, and K.Noda, Adv.Mater.20, 4442(2008).

[51] I.Meric, M.Y.Han, A.F.Young, B.Qzyilmaz, P.Kim, and K.L.Shepard, Nat. Nanotechnol. 3, 654(2008).

[52] A.K.Feldman, M.L.Steigerwald, and X.F.Guo, Acc. Chem. Res. 41, 1731(2008).

[53] P.Sharma and P.Ahuja, Mater. Res. Bull. 43, 2517(2008).

[54] P.Avouri, Z.H.Chen, and V.Perebeinos, Nat. Nanotechnol.2, 605(2007).

[55] R.S.Ruoff and D.C.Lorents, Carbon 33,925(1995).

[56] M.F.Yu, O.Lourie, M.J.Dyer, K.Moloni, T.F.Kelly, and R.S.Ruoff, Science 287, 637(2000).

[57] C.S.Lu, Appl. Phys. Lett. 92. 206101(2008).

[58] J.J.George, R.Sengupta, and K. Bhowmick, J. Nanosci. Nanotechnol. 8, 1913(2008).

[59] B.W.Jeong, J.K.Lim, and S.B.Sinnott, Appl. Phys. Lett. 90. 023102(2007).

[60] K.S.V.Santhanam and G.Lei, Encyclopedia, Nanoscience and Nanotechnology (2009).

[61] D.Tasis, N.Tagmatarchis, A.Bianco, and M.Prato, Chem. Rev. 106, 1105(2006).

[62] S.B Fagan and R.Mota, Phys.Rev. B 67, 2054(2003).

[63] S.B Fagan, R.Mota, J.R.Antonio, and A.Fazzio, Ohysica B 340, 982(2003).

[64] N.Rawat, R.Gudyaka, M.Kumar, B.Joshi, and K.S.V.Santhanam, J. Nanosci. Nanotechnol. 8, 2044(2008).

[65] M.Kumar, N.Rawat, and K.S.V.Santhanam, Mat. Res. Symposium (2006), 899E, 0899.

[66] Y.Yagi, T.M.Briere, M.H.F.Sluiter, V.Kumar, A.A.Farajian, and Y.Kawazoe, Phys. Rev. B 69, 75411(2004).

[67] Y.H.Chen and D.C.Jiles, IEEE Transactions on Magnetics 37, 2001.

[68] C.G.Beck and A.T.Santhanam, Scripta Metallurgica 12, 255(1978).

[69] I. Watanabe and C.Wallace, Open Dentistry J.2, 109(2008).

[70] B. Bozzini, G.P.De Gaudenzi, M.Serra, A.Fanigliulo, and F.Bogani, Mater.Corros.53, 328(2002).

[71] T.Stenberg and B.Bergman, Acta Odontologica Scadinavica 41, 14954(1983).

[72] N. Yang, Wuji Feijinshu Cailiao Ceshi Fangfa. Hubei China, Wuhan: Wuhan University of Technology Press (2005).

[73] K.R. Manrikkannu, G. P. Kalaignan and T. Vasudevan, J. Alloys and Compounds, 438, 332 (2007)